Final Technical Report

DTIC
ELECTE
JAN 2 3 1995
C
D
S

Nitride Semiconductors for Ultraviolet Detection

R. F. Davis, M. D. Bremser, D. Hanser,
K. Linthicum, B. Perry, and L. Smith
Materials Science and Engineering Department
North Carolina State University
Campus Box 7907
Raleigh, NC 27695-7907

19960117 085

December, 1995

REPORT DOCUMENTATION PAGE

Public reporting burden for this collection of information is estimated to average 1 hour per response, including the time for reviewing instructions, searching existing data sources, gathering and maintaining the data needed, and completing and reviewing the collection of information. Send comments regarding this burden estimate or any other aspect of this collection of information, including suggestions for reducing this burden, to Washington Headquarters Services, Directorate for Information Operations and Reports, 1215 Jefferson Davis Highway, Suite 1204, Arlington, VA 22202-4302, and to the Office of Management and Budget Paperwork Reduction Project (0704-0188), Washington, DC 20503.

1. AGENCY USE ONLY (Leave blank)	2. REPORT DATE December, 1995	3. REPORT TYPE AND DATES COVERED Final Technical 7/1/95–12/31/95

4. TITLE AND SUBTITLE

Nitride Semiconductors for Ultraviolet Detection

5. FUNDING NUMBERS

s400018srr01
1114SS
N00179
N66005
4B855

6. AUTHOR(S)

Robert F. Davis

7. PERFORMING ORGANIZATION NAME(S) AND ADDRESS(ES)

North Carolina State University
Hillsborough Street
Raleigh, NC 27695

8. PERFORMING ORGANIZATION REPORT NUMBER

N00014-92-J-1720

9. SPONSORING/MONITORING AGENCY NAMES(S) AND ADDRESS(ES)

Sponsoring: ONR, Code 312, 800 N. Quincy, Arlington, VA 22217-5660
Monitoring: Administrative Contracting Officer, Regional Office Atlanta
101 Marietta Tower, Suite 2805
101 Marietta Street
Atlanta, GA 30323-0008

10. SPONSORING/MONITORING AGENCY REPORT NUMBER

11. SUPPLEMENTARY NOTES

12a. DISTRIBUTION/AVAILABILITY STATEMENT

Approved for Public Release; Distribution Unlimited

12b. DISTRIBUTION CODE

13. ABSTRACT (Maximum 200 words)

Monocrystalline $Al_xGa_{1-x}N(0001)$ ($0.05 \leq x \leq 0.70$) thin films, void of oriented domain structures and low-angle boundaries and in the undoped, n-type Si doped ($x \leq 0.40$) and p-type Mg doped ($x \leq 0.13$) states have been grown via OMVPE directly on 6H-SiC substrates. The surface morphologies were smooth; the FWHM of the DCXRC curves (0002 reflection) were as low as 186 arc sec for the undoped films. Values of the bandgap as a function of composition showed a negative bowing parameter. A new OMVPE system devoted to growth and doping of $In_xGa_{1-x}N$ alloys and related alloys and a new method for gas source MBE of III-N materials at increased deposition rates have been commissioned. Temperature-dependent PL measurements of undoped GaN films indicated emission from both free and bound excitons. The exciton binding energy to the neutral donor was ≈ 7 meV. Photoluminescence at 4.2 K on a GaN film with a thickness gradient of .5 mm revealed an energy shift in the band-edge peak, most likely due to strain effects. Photoluminescence of GaN for thickness below .8 mm revealed an increase in the donor-acceptor pair (DAP) emission intensity which is tentatively attributed to an increase in acceptor doping. The use of HCl solutions to clean the surfaces of GaN(0001) yields the lowest O and C concentrations. As-deposited TiN contacts to Si-doped GaN with $n=7.4\times10^{18}$ cm^{-3} were ohmic with ρ_c at RT of 2.5×10^{-5} $\Omega\cdot$cm^2. On lower-doped GaN ($n=1.24\times10^{18}$ cm^{-3}) Ti and TiN contacts showed fairly high resistance in the as-deposited condition. However, they improved markedly as a result of annealing through 900°C. Contacts of Cu_3Ge/n-GaN also exhibited ohmic behavior, yielding an as-alloyed ρ_c of 18 $\Omega\cdot$cm^2 for $n=4.5\times10^{17}$ cm^{-3} and 4.9×10^{-3} $\Omega\cdot$cm^2 for $n=7.4\times10^{18}$ cm^{-3}. However, these contacts deteriorated substantially after annealing at 800°C. Platinum contacts on p-GaN:Mg were highly resistive in the as-deposited condition, but improved upon annealing through 800°C; after annealing at 900°C, resistance increased.

14. SUBJECT TERMS

AlGaN alloys, InGaN alloys, vapor phase epitaxy, molecular beam epitaxy, bowing parameter, X-ray rocking curves, photoluminescence, cathodoluminescence, free exciton, bound exciton, binding energy, band gap, carbon impurities, surface cleaning, HCl, ohmic contacts, TiN, Ti, Cu_3Ge, Pt, Au, Co

15. NUMBER OF PAGES

54

16. PRICE CODE

17. SECURITY CLASSIFICATION OF REPORT	18. SECURITY CLASSIFICATION OF THIS PAGE	19. SECURITY CLASSIFICATION OF ABSTRACT	20. LIMITATION OF ABSTRACT
UNCLAS	UNCLAS	UNCLAS	SAR

Table of Contents

I. Introduction

Continued development and commercialization of optoelectronic devices, including light-emitting diodes and semiconductor lasers produced from III–V gallium arsenide-based materials, has also generated interest in the much wider bandgap semiconductor mononitride materials containing aluminum, gallium, and indium. The majority of the studies have been conducted on pure gallium nitride thin films having the wurtzite structure, and this emphasis continues to the present day. Recent world-wide research has resulted in the fabrication of p–n junctions in wurtzitic gallium nitride, the deposition of cubic gallium nitride, as well as the fabrication of multilayer heterostructures, the formation of thin film solid solutions, p-n junction, double heterostructure and quantum well light emitting diodes and newly announced diode lasers. Chemical vapor deposition (CVD) has usually been the technique of choice for thin film fabrication. However, more recently these materials have also been deposited by plasma-assisted CVD and reactive and ionized molecular beam epitaxy.

The program objectives achieved in this reporting period have been (1) the deposition via OMVPE of monocrystalline $Al_xGa_{1-x}N(0001)$ ($0.05 \leq x \leq 0.70$) thin films, void of oriented domain structures and low-angle boundaries and in the undoped, n-type Si doped ($x \leq 0.40$) and p-type Mg doped ($x \leq 0.13$) states directly on 6H-SiC(0001) substrates and their characterization via photoluminescence, (2) the commissioning of a new OMVPE system for InGaN and associated alloys, growth and cathodoluminescence characterization of $Al_xGa_{1-x}N$ alloys and abrupt heterojunctions of these alloys, (3) the use of ammonia in an MBE environment for the growth of films of AlN, GaN and alloys of these materials, (4) temperature-dependent PL measurements of undoped GaN films, and (5) the investigation of Ti, TiN and Cu_3Ge as ohmic contacts to n-type GaN and Pt to p-type GaN.

The procedures, results, discussions of these results and conclusions of these studies are summarized in the following sections with reference to appropriate SDIO/ONR reports for details. Note that each major section is self-contained with its own figures, tables and references.

II. Growth and Doping of $Al_xGa_{1-x}N$ Deposited Directly on α(6H)-SiC(0001) Substrates Via Organometallic Vapor Phase Epitaxy

M. D. Bremser, W. G. Perry, N. V. Edwards, T. Zheleva, N. Parikh*, D. E. Aspnes**, R. F. Davis

Department of Materials Science and Engineering, North Carolina State University, Box 7907 Raleigh, NC 27695-7907
*Department of Physics and Astronomy, University of North Carolina at Chapel Hill, Chapel Hill, NC 27514
**Department of Physics, North Carolina State University, Raleigh, NC 27695-8202

ABSTRACT

Monocrystalline $Al_xGa_{1-x}N(0001)$ ($0.05 \leq x \leq 0.70$) thin films, void of oriented domain structures and associated low-angle grain boundaries, have been grown at high temperatures via OMVPE *directly on* vicinal and on-axis α(6H)-SiC(0001) wafers using TEG, TEA and ammonia in a cold-wall, vertical, pancake-style reactor. The surface morphologies were smooth and the densities and distributions of dislocations were comparable to that observed in GaN(0001) films grown on high temperature AlN buffer layers. Double-crystal XRC measurements showed a FWHM value as low as 186 arc sec for the (0002) reflection. Spectra obtained via CL showed strong near band-edge emissions with FWHM values as low as 31 meV. The compositions of the $Al_xGa_{1-x}N$ films were determined using EDX, AES and RBS and compared to the values of the bandgap as measured by spectral ellipsometry and CL emissions. A negative bowing parameter was found. Controlled n-type, Si-doping of $Al_xGa_{1-x}N$ for $x \leq 0.4$ has been achieved with net carrier concentrations ranging from $\approx 2\times10^{17}$ cm^{-3} to 2×10^{19} cm^{-3}. Acceptor doping with Mg for $x < 0.13$ was also successful.

A. Introduction

The numerous potential semiconductor applications of the wide bandgap III-Nitrides has prompted significant research regarding their growth and development. GaN (wurtzite structure), the most studied in this group, has a bandgap of $\approx$3.4 eV and forms continuous solid solutions with both AlN (6.2 eV) and InN (1.9 eV). As such, materials with engineered bandgaps are feasible for optoelectronic devices tunable in wavelength from the visible to the deep UV. The relatively strong atomic bonding of these materials also points to their potential for high-power and high-temperature microelectronic devices.

Single crystal wafers of GaN are not commercially available. Sapphire(0001) is the most commonly used substrate, although its lattice parameter and coefficients of thermal expansion are significantly different from that of any III-Nitride. The heteroepitaxial nucleation and growth of monocrystalline films of GaN on any substrate and AlN on sapphire are difficult at elevated (>900°C) temperatures. Therefore, at present, for successful organometallic vapor phase epitaxy (OMVPE) of GaN films on sapphire, the use of the initial deposition of an amorphous or polycrystalline buffer layer of AlN [1,2] or GaN [3,4] at low-temperatures (450°-600°C) is necessary to achieve both nucleation and relatively uniform coverage of the substrate surface. Subsequent deposition at higher temperatures and concomitant grain orientation competition has resulted in films of GaN(0001) and various nitride alloys of improved quality and surface morphology relative to that achieved by growth directly on this substrate.

By contrast, we have observed that AlN and $Al_xGa_{1-x}N$ alloys containing even low ($x \geq 0.05$) concentrations of AlN deposited on 6H-SiC(0001) substrates at high ($\geq$1000°C) temperatures undergo two-dimensional nucleation and growth with resulting uniform surface coverage. In our research, the use of a 1000 Å, monocrystalline, high-temperature (1100°C) AlN buffer has resulted in GaN films void of oriented domain structures and associated low-angle grain boundaries [5,6] Monocrystalline films of $Al_xGa_{1-x}N$ ($0.05 \leq x \leq 0.70$) of the same quality have also been achieved *directly on* 6H-SiC(0001) wafers at 1100°C. The presence of AlN in the films, the enhanced surface mobility of the adatoms at high temperatures and the reduced mismatch in lattice parameters between $Al_xGa_{1-x}N(0001)$ and 6H-SiC(0001) ($a/a_o \approx$1-3%) relative to that between $Al_xGa_{1-x}N$ and sapphire (11-13%) [2] have promoted the growth of these films [7]. The following is the first known published report of the deposition of undoped and doped high quality $Al_xGa_{1-x}N$ alloys without the use of a buffer layer.

B. Experimental Procedures

As-received vicinal 6H-SiC(0001) wafers [8] oriented 3°-4° off-axis toward <11$\bar{2}$0> were cut into 7.1 mm squares. These pieces were degreased in sequential ultrasonic baths of trichloroethylene, acetone and methanol and rinsed in deionized water. The SiC substrates were

3

then dipped into a 10% HF solution for 10 minutes to remove the thermally grown oxide layer and blown dry with N_2 before being loaded onto the SiC-coated graphite susceptor contained in a cold-wall, vertical, pancake-style, OMVPE deposition system. The system was evacuated to less than 3×10^{-5} Torr prior to initiating growth. The continuously rotating susceptor was RF inductively heated to the $Al_xGa_{1-x}N$ deposition temperature of 1100°C (optically measured on the susceptor) in 3 SLM of flowing H_2 diluent. Hydrogen was also used as the carrier gas for the various metalorganic precursors. Deposition of $Al_xGa_{1-x}N$ was initiated by flowing various ratios of triethylaluminum (TEA) and triethylgallium (TEG) in combination with ammonia (NH_3). The NH_3 and total metalorganic precursor flow rates were 1.5 SLM and 32.8 µmol/min, respectively. The system pressure was 45 Torr. Silicon doped n-type $Al_xGa_{1-x}N$ samples were achieved via the addition of SiH_4 (12.4 ppm in a balance of N_2) at flow rates between 0.05 nmol/min and 15 nmol/min. Magnesium doped p-type $Al_xGa_{1-x}N$ samples were achieved via the addition of Cp_2Mg at flow rates between 200 nmol/min and 400 nmol/min.

The structural, microstructural, optical and electrical characteristics of the epitaxial $Al_xGa_{1-x}N$ thin films were analyzed using several techniques. Scanning electron microscopy (SEM) was performed using a JEOL 6400FE operating at 5 kV which was equipped with an Oxford Light Element Energy Dispersive X-ray (EDX) Microanalyzer. Conventional and high resolution transmission electron microscopy (TEM) was conducted using a Topcon EM-002B microscope operating at 200 kV. Double-crystal x-ray rocking curve (DCXRC) measurements were made on a Philips MR3 thin films diffractometer. The catholuminescence (CL) properties of the $Al_xGa_{1-x}N$ films were determined at 4.2 K using a Kimball Physics EMG-14 electron gun as the excitation source. Spectral ellipsometry (SE) was performed using a rotating analyzer ellipsometer with a xenon arc lamp (1.5eV–5.75eV). Capacitance-Voltage (CV) measurements were conducted using a MDC Model CSM/2-VF6 equipped with a mercury probe. Auger electron spectroscopy (AES) was performed using a Perkin-Elmer Model 660 equipped with Zalar rotation. Rutherford backscattering analysis was performed using 1.9 MeV He^+ ions with the detector at an angle of 165°.

C. Results and Discussion

Previous research in our laboratories has shown that thin films of GaN deposited directly on 6H-SiC(0001) substrates at high and low temperatures had columnar-like grains, faceted surfaces and high net carrier concentrations ($n_D-n_A > 1\times10^{19}$ cm^{-3}) [9]. In contrast, in the present research monocrystalline thin films of $Al_xGa_{1-x}N$ (x ≤0.05) have been deposited directly on the same type of SiC substrates *without the use of a buffer layer* with no misorientation or low-angle grain boundaries, determined by selected area diffraction (SAD) and microstructural analysis via TEM. The stacking fault density was also very low. These results are apparent in

4

the representative cross-sectional TEM micrograph shown in Fig. 1a. Inserts in the micrograph show SAD patterns from the top layer of $Al_{0.13}Ga_{0.87}N$ and the film/substrate interface. Overlapping spots from the 6H-SiC(0001) substrate are seen in the latter pattern. The dislocation density of these films at the interface appears to similar to GaN films deposited on a high temperature (HT) buffer layer [5,6] The dislocation density of the $Al_xGa_{1-x}N$ film decreases rapidly as a function of thickness, as shown in Fig. 1a, and only threading dislocations which result from misfit dislocations at the interface persist through the film. High resolution TEM of the AlGaN/SiC interface is shown in Fig. 1b.
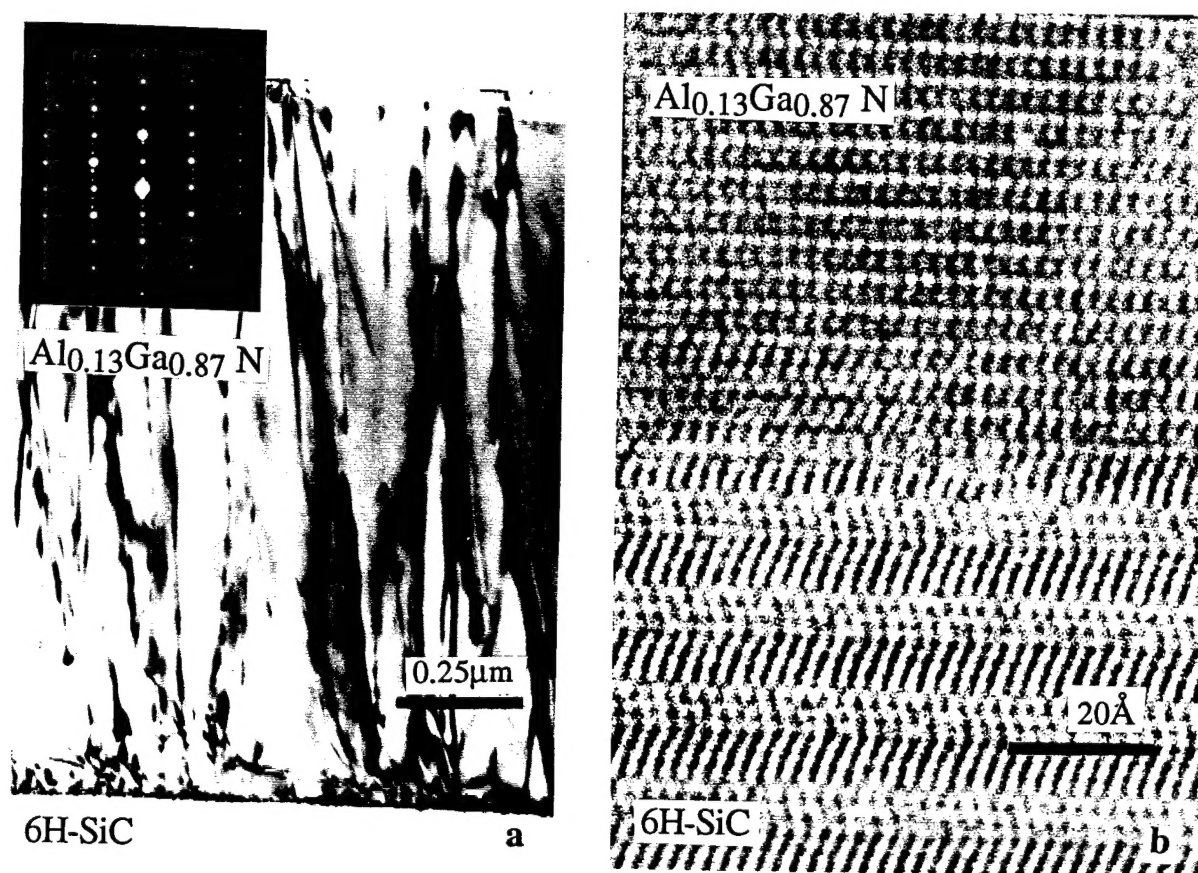

Figure 1.   a) Cross-sectional TEM micrograph of a 1.8 μm AlGaN(0001) film deposited at 1100°C and 45 Torr via OMVPE directly on a vicinal 6H-SiC(0001) substrate. The inset shows the selected area diffraction. b)High resolution TEM of the AlGaN/SiC interface

The surfaces of the $Al_xGa_{1-x}N$ films exhibited a slightly mottled appearance, as shown in Fig. 2, probably as a result of the step and terrace features on the growth surface of the vicinal 6H-SiC(0001) substrates. Random pinholes, caused by incomplete coalescence of the two dimensional islands which occurred as an intermediate growth stage between the initial nucleation and the final layer-by-layer growth stage representative of the majority of the film,

were also observed. For $Al_xGa_{1-x}N$ compositions for x > 0.5, a significant number of pinholes appeared on the surface. Based on previous work with GaN, the pinhole density can be decreased with increasing growth temperature due to the enhanced surface mobility of the adatoms at higher temperatures [5,6] The higher growth rate of films grown on off-axis material is due to the increased density of steps on the substrate and film. DCXRC measurements taken on the 1.8 μm $Al_{0.13}Ga_{0.87}N$ film shown in Fig. 1 revealed the FWHM of the (0002) reflection to be 186 arc sec. For a 0.9 μm film of the same composition, the FWHM value of the same reflection was 315 arc sec. The reduction in FWHM values is consistent with the decrease in alloy concentration.
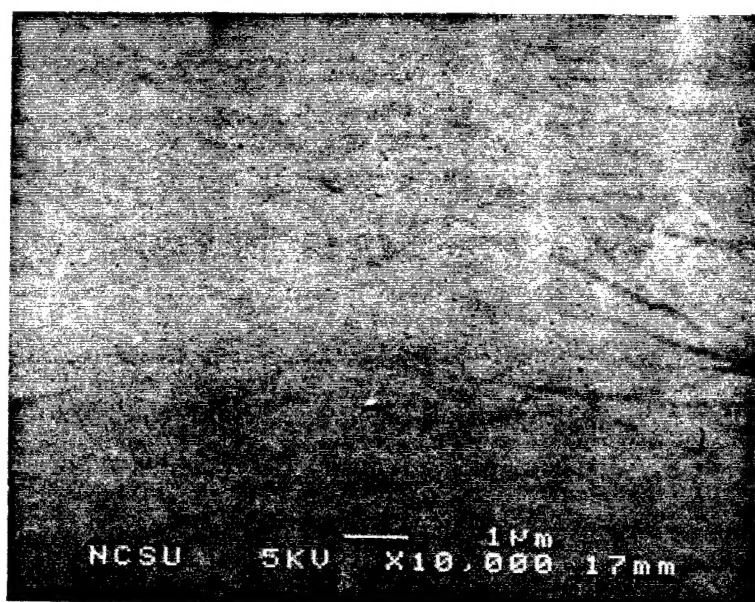

Figure 2.   Representative SEM micrograph of the surface of an AlGaN(0001) film similar to that shown in Fig. 1.

The low-temperature (4.2K) CL spectra of the undoped $Al_xGa_{1-x}N$ films for various compositions (0.05 ≤ x ≤ 0.70) revealed an intense near band-edge emission which has been attributed to an exciton bound to a neutral donor (I_2-line emission) [10,11]. Broadening of this emission is attributed to both exciton scattering in the alloys, as well as small variations in alloy composition in the film. The lowest FWHM value observed for the $Al_xGa_{1-x}N$ alloys was 31 meV. Strong defect peaks, previously ascribed to donor-acceptor pair recombination [12], were observed at midgap energies. The broad peak centered at 545 nm (2.2 eV) for GaN, commonly associated [13] with deep-levels (DL) in the bandgap, was also observed; however, these emissions shifted sublinearly with changing composition. The nature of this behavior is under investigation.

The compositions of seven films grown under different conditions were determined using EDX, AES and RBS. Standards of AlN and GaN grown in the same reactor under similar conditions were used for the EDX and AES analyses. After careful consideration of the errors (± 3 at.%) involved with each technique, compositions were assigned to each film. The data from EDX and AES measurements showed excellent agreement. The RBS data did not agree as well with the other two techniques due to small compositional variations through the thickness of the film. Simulation of the composition determined by RBS was conducted only on the surface composition. Analysis via EDX revealed that the $Al_xGa_{1-x}N$ grown on the on-axis SiC substrates tended to be slightly more Al rich than those grown off-axis SiC. It is thought that the presence of steps on the growth surface favors the adhesion of the gallium adatoms. In all cases except one, this difference was less than 2 atomic percent. Under the most aluminum rich growth conditions, the difference was 6-8 atomic percent. This difference was revealed by all three techniques. At this time, the reason for this large difference is unclear.

In Figs. 3 and 4, these compositions are compared with their respective CL emission peaks and bandgap as determined by SE. Using a parabolic model, the following relationships describe the bandgap (Eq. 1) and CL (I_2-line emission) (Eq. 2) as a function aluminum mole fraction for $0 \leq x \leq 0.70$:
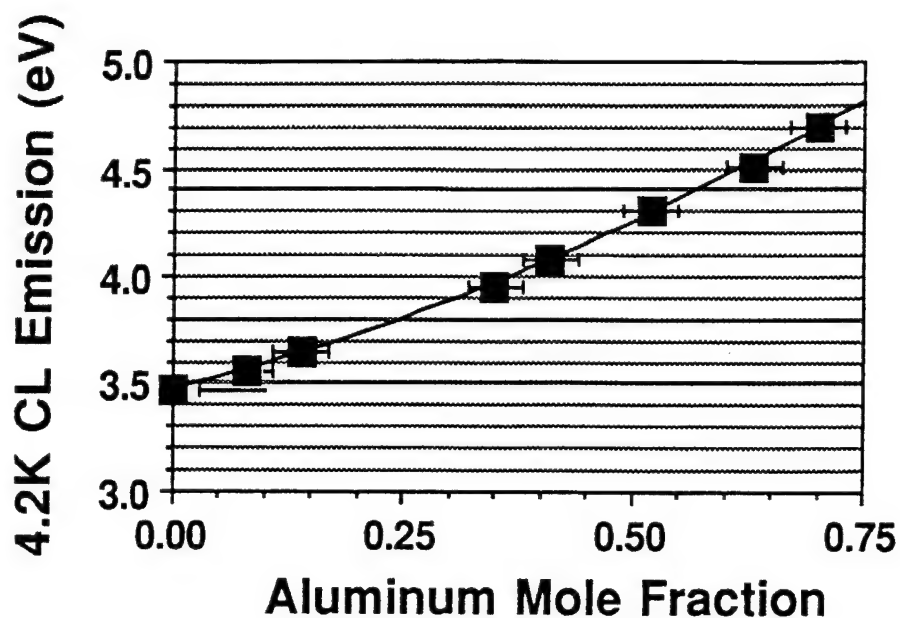
$$E_g(x) = 3.40 + 1.35x + 1.01x^2, \tag{1}$$

$$E_{I2}(x) = 3.47 + 1.07x + 0.96x^2. \tag{2}$$

Clearly, both measurements show a negative deviation from a linear fit. This is in agreement with earlier research by other investigators [10,11].

Undoped, high quality $Al_{0.05}Ga_{0.95}N$ films grown directly on vicinal 6H-SiC(0001) exhibited residual, n-type background carrier concentrations of $\leq 1\times10^{18}cm^{-3}$. The carrier concentration rapidly decreased with increasing Al content and was $<1\times10^{16}cm^{-3}$ for $Al_{0.35}Ga_{0.65}N$, as determined by CV measurements. The origin of this residual carrier concentration is under investigation, since concentrations of $<1\times10^{15}$ cm^{-3} have been measured for GaN films grown on AlN buffer layers in the same reactor. However, the controlled introduction of SiH_4 allowed the reproducible achievement of donor carrier concentrations within the range of 2×10^{17} cm^{-3} to 2×10^{19} cm^{-3} in films with $x \leq 0.4$. The growth of p-type $Al_xGa_{1-x}N$ films for $x \leq 0.13$ via the introduction of Mg has been successful. All attempts to similarly dope films with $x > 0.13$ have been unsuccessful.

D. Conclusions

$Al_xGa_{1-x}N(0001)$ ($0.05 \leq x \leq 0.70$) thin films void of low-angle grain boundaries and resultant domain microstructures have been grown via OMVPE directly on vicinal and on-axis

$$CL = 3.47 + 1.07x + 0.96x^2$$
$$R^2 = 0.999$$

Figure 3.   Low-temperature (4.2K) CL emissions of $Al_xGa_{1-x}N$ films as a function of aluminum mole fraction.
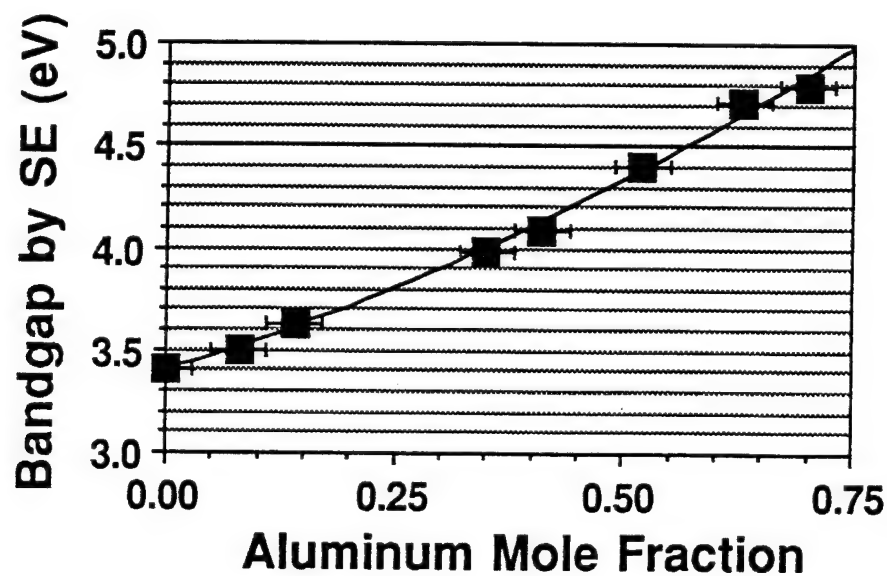
$$BG = 3.40 + 1.35x + 1.01x^2$$
$$R^2 = 0.995$$

Figure 4.   Bandgaps measured by spectral ellipsometry of $Al_xGa_{1-x}N$ films as a function of aluminum mole fraction.

α(6H)-SiC(0001) substrates. A significant reduction in dislocation density with increasing thicknesses was observed via TEM. Low-temperature CL spectra of the films showed intense near band-edge emissions. For a 1.8 μm $Al_xGa_{1-x}N$ film (x=0.13), DCXRC measurements revealed a FWHM value of 186 arc sec for the GaN(0002) reflection. The composition of the $Al_xGa_{1-x}N$ films was determined using EDX, AES and RBS and compared to the values of the bandgap measured by spectral ellipsometry and CL emissions. A negative bowing parameter was found. Controlled n-type Si-doping of $Al_xGa_{1-x}N$ has been achieved for net carrier concentrations ranging from $\approx 2\times10^{17}$ cm^{-3} to $\approx 2\times10^{19}$ cm^{-3} for x $\leq$ 0.4. The p-type doping with Mg of $Al_xGa_{1-x}N$ for x < 0.13 has also been successful.

E.   Acknowledgments

F.   References

1.   M. A. Khan, J. N. Kuznia, D. T. Olson and R. Kaplan, J. Appl. Phys. **73**, 3108 (1993).
2.   H. Amano, I. Akasaki, K. Hiramatsu, N. Koide and N. Sawaki, Thin Solid Films **163**, 415 (1988).
3.   J. N. Kuznia, M. A. Khan, D. T. Olson, R. Kaplan and J. Freitas, J. Appl. Phys. **73**, 4700 (1993).
4.   S. Nakamura, Jpn. J. Appl. Phys. **30**, L1705 (1991).
5.   T. W. Weeks, Jr., M. D. Bremser, K. S. Ailey, E. P. Carlson, W. G. Perry, R. F. Davis, Appl. Phys. Lett. **67**, 401 (1995)
6.   T. W. Weeks, Jr., M. D. Bremser, K. S. Ailey, W. G. Perry, E. P. Carlson, E. L. Piner, N. A. El-Masry, R. F. Davis, J. Mat. Res. to be published.
7.   R. F. Davis T. W. Weeks, Jr., M. D. Bremser, K. S. Ailey, W. G. Perry, Z. Sitar, C. Wang and K. Linthicum, Topical Workshop on III-V Nitrides, Nagoya, Japan, September 21-23 (1995).
8.   Cree Research, Inc., 2810 Meridian Parkway, Suite 176, Durham, NC 27713.
9.   T. W. Weeks, Jr., D. W. Kum, E. Carlson, W. G. Perry, K. S. Ailey and R. F. Davis, Second International High Temperature Electronics Conference, Charlotte, NC, June 5-10 (1994).
10.   M. R. H. Khan, Y. Koide, H. Itoh, N. Sawaki, I. Akasaki, Solid State Commun. **60** 753, (1986).
11.   B. V. Baranov, V. B Gutan U. Zhumakulev, Sov. Phys.-Semicond. **16**, 819, (1982).
12.   R. Dingle and M. Ilegems, Solid State Commun. **9**, 175 (1971).
13.   W. Götz, N. M. Johnson, R. A. Street, H. Amano and I. Akasaki, Appl. Phys. Lett. **66**, 1340 (1995).

APPENDIX

In addition to growth research in the area of $Al_xGa_{1-x}N$, an ongoing effort is in place to further optimize and improve the growth of GaN. Much of this work is driven by the need to overcome challenges presented by device design.

A. Optimization of Deposition Temperature

Growth of GaN at different temperatures was investigated using a 1000Å AlN buffer deposited at 1100°C prior GaN deposition. This is a continuation of earlier work on GaN deposition. GaN was deposited in the 950°C to 1200°C temperature range. Below 1100°C, the growth rate was constant with increasing deposition temperature, thereby indicating a diffusion limited process. At 1100°C, a significant reduction in the growth rate was observed indicating a marked increase in GaN desorption during growth. Above 1100°C, very little GaN was deposited. Therefore, 1050°C has been chosen as the preferred deposition temperature due to its strong near-band edge photoluminscence (PL) emission at 4.2K, smooth pit-free surfaces, low double crystal x-ray rocking curves (DCXRC), full width at half-maximums (FWHM) and repeatedly n-type background carrier concentrations below 1×10^{16} cm^{-3}.

B. Buffer Layer Elimination

Previous research showed that deposition of GaN directly on 6H-SiC resulted in low quality films with a columnar structure; however, only deposition in the range of 500-950°C was investigated. In an attempt to eliminate growth of the AlN buffer layer, GaN was deposited directly on SiC at temperatures of 1100°C to 1200°C, but no significant amount of GaN nucleated on the surface of the SiC. Based on the deposition of AlGaN directly on SiC and the ability to dope $Al_xGa_{1-x}N$ n-type for x<0.4, it is believed that the development of a conducting $Al_xGa_{1-x}N$ buffer layer for small x is possible. This would facilitate the use of backside contacts for vertical device structures, as well as minimize the band offset between the SiC substrate and the buffer layer.

C. Full Wafer Deposition

In order to meet the needs of several characterization techniques, several samples of GaN were deposited on whole 30 mm SiC wafers under normal deposition conditions. During this deposition, the temperature variation across the samples was measured to be less than 5°C using an Ircon IMAX infrared optical pyrometer. The difference in the susceptor temperature and wafer temperature was measured to be about 35°C. The thickness varied from 3.71 μm at the center of the sample to 3.61 μm at the edge. This corresponds to a thickness varience of less than 3% across the sample. The uniformity in growth temperature and thickness will be important for the deposition of device structures.

D. Atomic Force Microscopy Studies

Preliminary studies of the roughness of GaN surface grown by OMVPE have been undertaken. GaN grown on on-axis SiC substrates has been repeatedly shown to have a root mean squared (RMS) roughness of < 2Å for a 1 μm square area, while simultaneously deposited GaN on off-axis SiC has a RMS roughness in the range of 10-20Å. However, it should be noted that larger area scans of GaN on off-axis substrate showed large parallel ridge-like features which vertical dimension in excess of 50Å. Corresponding on-axis material did not exhibit these structures.

Both off-axis and on-axis SiC substrates were also examined as received from Cree Research. The off-axis SiC substrates had a RMS roughness of <5Å over a 5 μm square area while the on-axis SiC exhibited a RMS roughness of 11 Å for the same size area. It should be noted that the off-axis wafers have ~ 1 μm epitaxial layer of SiC on them while the on-axis wafers do not. Interestly, on a typical on-axis wafer most of the wafer is extremely flat except for randomly oriented trenches with depths as great as 100 Å which probably are the result of the mechanical polishing of the wafers.

This work is preliminary, but provides some insight into the nature of the surface upon contacts for device will be placed, as well as lend itself to quantification damage due to etching of the material during device fabrication.

E. Acknowledgments

Davis Group:

- B. Perry—PL, CL, X-Ray analysis
- T. Zheleva—TEM , X-Ray analysis
- E. Carlson and D. Bray—ion implantation
- S. King—surface cleaning and analysis
- L. Smith and K. Tracy—contacts
- S. Smith and S. King—etching
- M. Behbehani and B. Therrien—device fabrication

III. Growth of GaN and InGaN Thin Films on $\alpha(6H)$-SiC(0001) Via Organometallic Vapor Phase Epitaxy

A. Introduction

With recent world-wide research efforts, the III-V nitride compounds have shown their potential for optoelectronic and microelectronic semiconductor device applications. The advancements in film quality and the understanding of materials issues have led to the demonstration and production of high quality LEDs. High power, high brightness LEDs with emission spectra ranging from yellow to violet have been produced [1-5]. Using a single quantum well heterostructure, Nakamura *et al.* have produced a blue LED with 4 mW power output at 20 mA with a 7.3% external quantum efficiency [5]. There has also been much recent progress in lasing and stimulated emission in GaN and InGaN. Amano *et al.* have shown violet stimulated emission from a photopumped AlGaN/InGaN heterostructure, demonstrating optical confinement and the feasibility of laser structures in this material system [6]. Although progress has been made in both optoelectronic and microelectronic devices, further developments are possible. Achieving an electrically pumped laser diode is one of the current major goals of the world-wide research effort in the III-V nitrides. To further investigate and demonstrate the capabilities of these materials, our research group developed and built a novel organometallic vapor phase epitaxy system. Progress made in the growth of GaN and InGaN films will be discussed in this report.

B. Experimental Procedure

An inverted flow rotating disc OMVPE system was used to grow the nitride films. The design and features of the system have been described in detail in a previous report [7]. The reactants used in the film growth were trimethylaluminum (TMA), triethylgallium (TEG), trimethylindium (TMI) and ammonia (NH_3). Hydrogen was used as the diluent and carrier gas. The system was operated under both manual and computer control.

The films were grown on Si-face SiC(0001) substrates cut 3-4° off-axis towards the $<11\bar{2}0>$. The as-received wafers were cut using a diamond saw into 7mm square pieces and degreased. The SiC pieces were then dipped into a 10% HF solution for 10 minutes to remove the thermally grown oxide and then blown dry with N_2. The substrates were then mounted on the SiC-coated graphite substrate holder and loaded in the system. The reactor chamber was evacuated to less than 2×10^{-6} torr before initiating growth. The substrate was heated to the deposition temperature in 2000 sccm of flowing H_2 diluent. In addition, 20 sccm of H_2 was flowed continuously through the radial precursor mixing manifold, which acted as a purge between gas source switching. The deposition pressure was 45 torr. The substrate holder was rotated continuously at approximately 45 rpm. The temperature of the substrate holder was measured using an Ircon Ultimax Infrared Thermometer and varied with the film being

deposited. While the growth temperature was being obtained, the flow of the carrier gas through the metalorganic bubblers was established. The temperature and pressure of each metalorganic bubbler was independently controlled.

Once the growth temperature was reached, film deposition was started by flowing the metalorganic precursor(s) and NH_3 into the reactor. For GaN growth, a high temperature AlN buffer layer was used. Once the growth temperature of 1100°C was reached, AlN deposition was started by flowing TMA and NH_3 into the reactor at 12.7 μmol/min and 1500 sccm, respectively. The AlN buffer layer was grown for 5 minutes corresponding to a thickness of approximately 1000 Å. After 5 minutes, the TMA flow was switched off and the temperature was lowered to 1000°C. Once this temperature was obtained, GaN deposition was started by flowing TEG into the reactor at a rate of 23.7 μmol/min. After the prescribed time, the TEG flow was switched off and the film was cooled to room temperature in flowing H_2 and NH_3. The growth rate of the GaN film was approximately 5 μm/hour.

For the InGaN growth a low temperature GaN buffer layer was used. At a temperature of 600°C, GaN deposition was started by flowing TEG and NH_3 into the reactor at 1.0 to 2.0 μmol/min and 1250 sccm, respectively. The GaN was grown for 15 minutes. After the prescribed time, the TEG flow was switched off and the substrate holder temperature was increased to 800°C to grow the InGaN. Varying growth conditions were investigated. The V/III ratio was varied from 3000 to 8000 and the TMI/TEG (molar flow per minute ratio) value was varied from 2 to 7.5. The InGaN films were grown for one hour.

The photoluminescence (PL) properties of the films were determined at 4.2 K using a 15 mW He-Cd laser (λ=325 nm) as the excitation source. The Double-Crystal X-ray Rocking Curve (DCXRC) measurements were made on a Bede Scientific Model 200 double crystal diffractometer using Cu $K\alpha_1$ radiation. Scanning Electron Microscopy (SEM) was performed on a JEOL 6400 FE operating at 5 kV.

C. Results and Discussion

GaN Growth. Figures 1 and 2 are SEM micrographs representative of the quality of the preliminary growth of AlN and GaN films, respectively. The AlN film has few distinguishable features on the relatively flat surface. Deposition of a flat, monocrystalline buffer layer is necessary in order to deposit high quality GaN films [8]. SiC has an advantage over sapphire in this respect, since monocrystalline AlN films can be deposited directly on SiC at high temperatures. On sapphire, AlN is deposited at low temperatures as an amorphous or finely-grained layer which then recrystallizes at higher temperatures [9-11]. These crystallized films on sapphire have been shown to be highly oriented polycrystals with low-angle grain boundaries and misoriented by ≈3° in the basal plane relative to the substrate. This leads to a large number of threading dislocations, estimated to be around 10^{10} cm^{-2} [11]. On SiC, the

dislocation density of GaN grown on a high temperature AlN buffer layer is at least one order of magnitude lower [8]. While the initial results in this study are promising, the AlN buffer layer growth parameters will be further optimized and the buffer layer structure will be investigated using high-resolution transmission electron microscopy (HRTEM). Other buffer layers including AlGaN, graded layers, and superlattices will also be investigated.
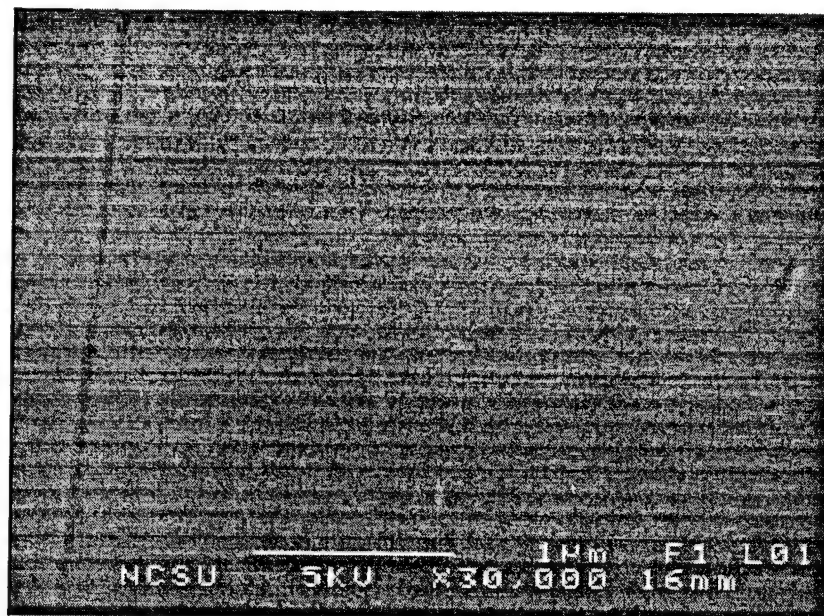

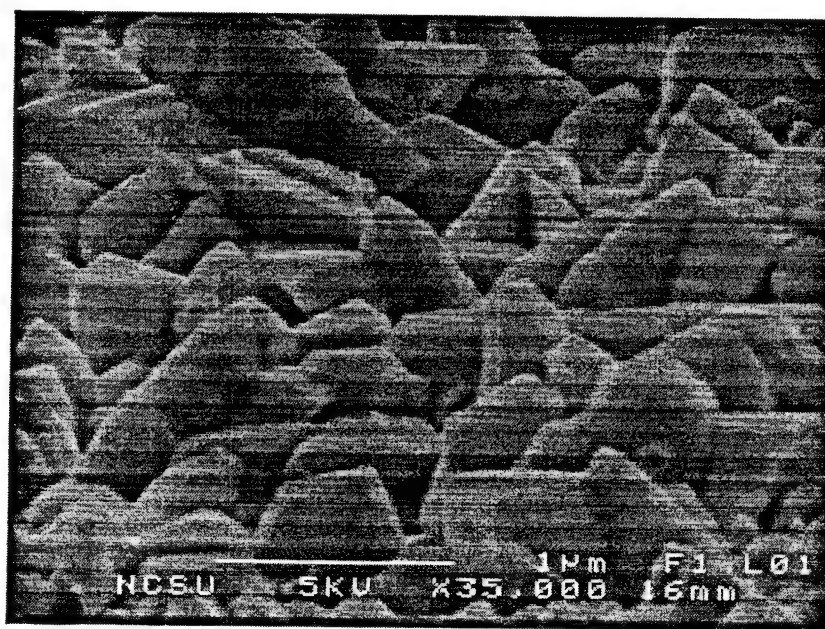Figure 1.   SEM micrograph of surface of AlN film.

Figure 2.   SEM micrograph of surface of GaN film.

Figure 2 shows the random polycrystalline nature of the GaN film grown on a typical AlN buffer layer in Fig. 1. The morphology of the film is attributed to the high growth rate of the GaN film (approximately 5 μm/hour). Reducing the growth rate the GaN should yield smoother films, reflecting the high quality of the AlN buffer layer. Further optimization of the growth parameters will be investigated.

InGaN Growth. In this study, the InGaN films were grown on a low temperature GaN buffer layer to determine film growth parameters. In growing the films, the V/III ratio was varied from 3000 to 10000 and the TMI/TEG molar ratio was varied from 2 to 7.5. At low V/III ratios (< 8000) the deposited films had a mottled appearance and were non-reflective.

Using an optical microscope metal droplets were visible on the surface. However, at a V/III ratio of 8000 and higher, the films were highly reflective and no metal droplets were evident on the film surface when viewed under the optical microscope.

Using a V/III ratio of 8000 and a deposition temperature of 800°C, the effect of varying the TMI/TEG ratio was investigated. At TMI/TEG value of 2, no indium was incorporated into the films as measured by PL and DCXRC measurements. At TMI/TEG values of 3 and higher, there was evidence of indium incorporation. Figure 3 shows the PL spectra at 4.2 K of InGaN film grown at a TMI/TEG value of 3. The near band edge emission peak is centered at 363.8 nm. Using the following equation

$$E_g(X) = XE_{g,InN} + (1-X)E_{g,GaN} - bX(1-X),$$

where $E_g(X)$ is the bandgap of the InGaN alloy with In mole fraction X, $E_{g,InN}$ is the bandgap of InN, taken to be 1.95 eV, $E_{g,GaN}$ is the bandgap of GaN, taken to be 3.54 eV, and b is the bowing parameter, taken to be 1.00 eV [12], the percent In in the alloy is 3.7% Typical DCXRC full width at half maximum (FWHM) values are between 300 and 500 arcsec for the In-containing compounds.

A better template for the InGaN growth would be a thick GaN film grown on a high temperature AlN buffer layer. However, at this time the GaN film growth has not been optimized and cannot be used as a template layer. As the GaN growth progresses and film quality increases, InGaN will be grown on thick GaN layers.

D.   Conclusions

The growth of AlN and GaN films on Si-face SiC(0001) using a novel OMVPE system design has been investigated. SEM micrographs show relatively flat AlN films and random polycrystalline GaN films. The polycrystalline nature of the GaN films is due to the high growth rate of the film. InGaN film growth has also been investigated. V/III ratios above 8000

give highly reflective films with smooth surfaces. TMI/TEG ratios above 3 show indium incorporation in the films as measured by PL and DCXRC measurements.
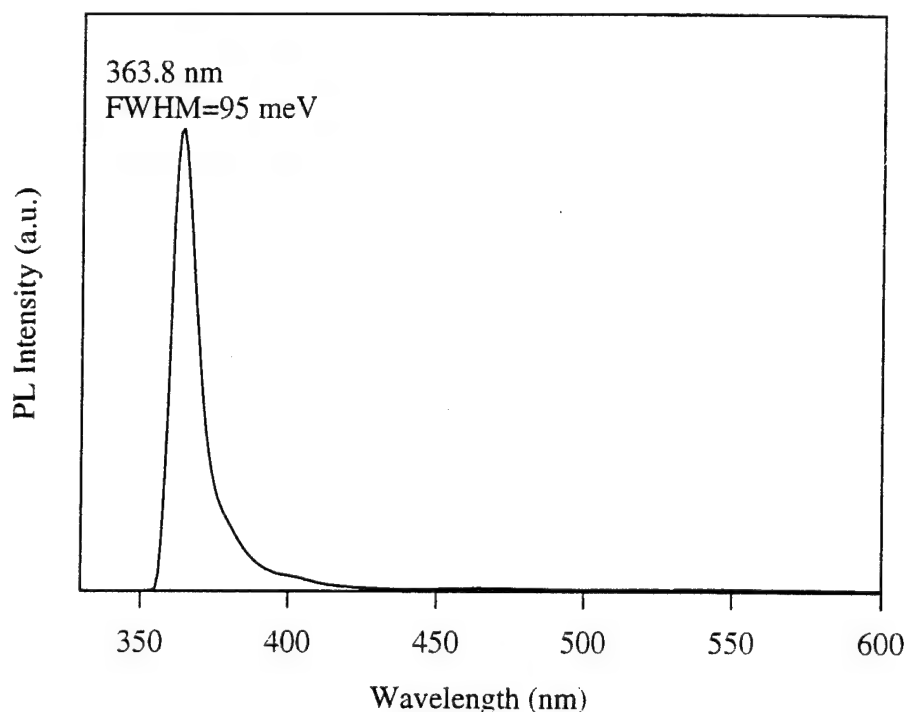
Figure 3. PL spectra of InGaN alloy grown with a TMI/TEG value of 3. Indium content is calculated to be 3.7%. Measurement taken at 4.2 K.

E. References

1. S. Nakamura, T. Mukai, and M. Senoh, Appl. Phys. Let. **64** (13), 1687 (1995).
2. S. Nakamura, J. Cryst. Growth **145**, 911 (1994).
3. M. A. Khan, Q. Chen, R. A. Skogman, and J. N. Kuznia, Appl. Phys. Let. **66** (16), 2046 (1995).
4. S. Nakamura, T. Mukai, and M. Senoh, J. Appl. Phys. **76** (12), 8189 (1994).
5. S. Nakamura, M. Senoh, N. Iwasa, and S. Nagahama, Jpn. J. Appl. Phys. **34**, L797 (1995).
6. H. Amano, T. Tanaka, Y. Kuni, K. Kato, S. Kim, and I. Akasaki. Appl. Phys. Let. **61** (11), 1377 (1994).
7. Nitride Semiconductors for Ultraviolet Detection, Semiannual Report, 1994.
8. T. W. Weeks, M. D. Bremser, K. S. Ailey, E. Carlson, W. G. Perry, and R. F. Davis, Appl. Phys. Let. **67** (3), (1995).
9. S. Tanaka, R. S. Kern, and R. F. Davis, Appl. Phys. Let. **66** (1), 37 (1995).
10. K. Hiramatsu, S. Itoh, H. Amano, I. Akasaki, N. Kuwano, T. Shirashi, K. Oki. J Cryst. Growth **115**, 628 (1991).
11. W. Qian, M. Skowronski, M. De Graef, K. Doverspike, L. B. Rowland, and D. K. Gaskill, Appl. Phys. Let. **66** (10), 1252 (1995).
12. S. Nakamura, N. Iwasa, and S. Nagahama, Jpn. J. Appl Phys. **32,** Pt. 2, No. 3A, L338 (1993).

IV. The Use of NH$_2$ for Film Growth

A. Introduction

AlN, GaN and InN thin films are presently grown by various techniques including metalorganic vapor phase epitaxy (MOVPE), RF sputtering, and molecular beam epitaxy (MBE). Currently, MOVPE has played the dominate role in nitride based wide bandgap device development. MBE growth of the III-V nitrides has until recently predominately used nitrogen electron cyclotron resonance (ECR) plasma assisted GSMBE. One of the major consequences of using ECR plasmas is the resulting ion damage occurring during film growth. It is generally believed now that, as a result of the low bond strength of the surface and near-surface atoms of GaN and InN, there is an increased potential for point defect damage and resulting electrical compensation in these materials. This damage would arise from the interaction of high energy N species with the surface and near-surface regions of these materials during deposition [1-3]. This is especially true if the plasma power is increased to enhance the flux of the reactive species. Recent research has shown that GaN films grown at higher microwave powers exhibit degraded electrical and luminescent properties as compared to films grown at lower microwave power levels [4-7]. Therefore, an alternative method of producing atomic nitrogen that minimizes or eliminates the undesirable production of high energy ionic nitrogen is needed.

Currently, there are two alternative methods being researched to address this concern. The first method employs the use of a radio frequency (RF) plasma source [3,8-10]. This source is found to emit a much larger fraction of atomic nitrogen and 1st-positive series excited molecular nitrogen than the ECR source [3]. The second method uses ammonia (NH$_3$) as the source of nitrogen [10,11]. Methods of cracking the ammonia include precracking in cracker cells, cracking on the substrate surface, and by employing reactive ion MBE (RIMBE) to produce low-energy NH$_x^+$ ions. This report presents the growth of GaN and AlN using thermally cracked NH$_3$ as the nitrogen source as an alternative to the ECR source in GSMBE.

B. Experimental Procedure

Two methods of cracking the ammonia are investigated in this report. The first is by cracking directly on the substrate surface and the second by precracking in an ammonia cracker. The ammonia cracking source manufactured by Effusion Science Inc. is installed in the sleeve of our currently unused MBE effusion cell (2.25" diameter). Nitride-grade ammonia is used as the source gas and is further purified by a Nanochem ammonia purifier prior to entering the cracker cell. A 0-10 SCCM flow controller is used to adjust the ammonia flux. After entering the cracker cell, the ammonia is decomposed by means of a single bounce delivery off of a wide-area catalytic rhenium filament. Al and Ga fluxes are provided by the normal MBE effusion cells.

A quadrupole mass spectrometer was used to characterize the resulting flux exiting the cracker cell under various filament temperatures and ammonia flow rates. GaN and AlN were then grown using various growth temperatures and III/V flux ratios with and without precracking of the ammonia in the cracker cell. The microstructures of the films were characterized by reflection high energy electron diffraction (RHEED), scanning electron microscopy (SEM) and photoluminescence (PL) analyses.

C. Discussion

The use of cracking ammonia as a source of nitrogen is not new to the field of III-V nitride growth. It is the current method used in growth techniques such as MOCVD and MOVPE where ammonia is cracked on the surface of the substrate, requiring relatively higher growth temperatures to achieve efficient nitrogen production. Several recent successes have been reported in the use of GSMBE utilizing Ga and NH_3 to grow GaN on sapphire substrates [10-15]. Reactive molecular beam epitaxy has also used the cracking of ammonia on the substrate as a nitrogen source [16,17]. Another technique recently used was hot filament enhanced CVD [18,19]. In this process, it is surmised that the catalyzed film growth is initiated through the decomposition of ammonia and subsequent production of NH radicals by a heated tungsten filament. These products trigger further reactions which react with the metalorganic gas to form precursors to film deposition. These precursors then decompose on the heated substrate resulting in film growth [19]. The decomposition of ammonia on various filament surfaces at high temperatures has shown that the two primary reactions that occur are:

$$NH_3 + M \rightarrow NH_2 + H + M \tag{1}$$

$$NH_3 + H \rightarrow NH_2 + H_2 \tag{2}$$

In the case of the catalyzed CVD growth, reaction 2 is enhanced by the addition of hydrogen to the reaction chamber between the tungsten filament and the heated substrate to aid in the production of NH_2. It is the secondary reactions, primarily the formation of NH radicals, that next occur which are responsible for precursor formation with the metalorganic mentioned above [18-20]. Examples of these secondary reactions include:

$$NH_2 + H \rightarrow NH + H_2 \tag{3}$$

$$NH_2 + NH_2 \rightarrow NH + NH_3 \tag{4}$$

Ammonia Gas Cracker Design. The ammonia cracker was designed to allow the ammonia to decompose primarily to NH_2 while limiting the formation of N_2 by means of a single interaction with a wide-area catalytic Re filament [18,19]. Rhenium was chosen for two

reasons: (1) rhenium catalysts are exceptionally resistant to passivation from gases such as nitrogen [21] and (2) hydrogen atoms have been detected in ammonia decomposition reactions on rhenium filaments heated to high temperatures approaching 2000 K [22]. Therefore, it should not be necessary to add hydrogen from some other source to aid in the production of NH_2. Secondary reactions on the substrate surface will produce NH radicals which are highly reactive with the group III species and result in film growth.

Ammonia Gas Cracker Characterization. The ammonia gas cracker was tested to determine which combination of filament temperature and ammonia flow rate would provide the most efficient source of atomic nitrogen and NH radicals needed for III-V nitride growth. The temperature of the Rhenium filament is measured indirectly by using I-V versus temperature data provided by Effusion Science, Inc. Mass spectrometry was used to measure the resulting mass current intensities resulting from various operating parameters. An example of this data is shown in Fig. 1. Figures 2-4 show the various ratios of mass intensities to that of ammonia.
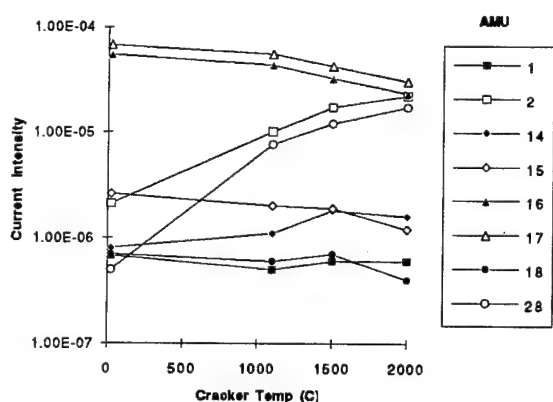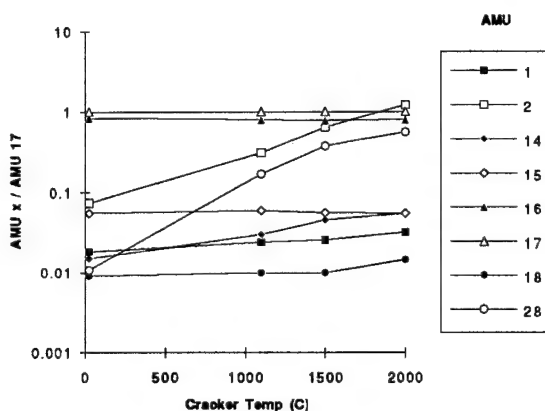
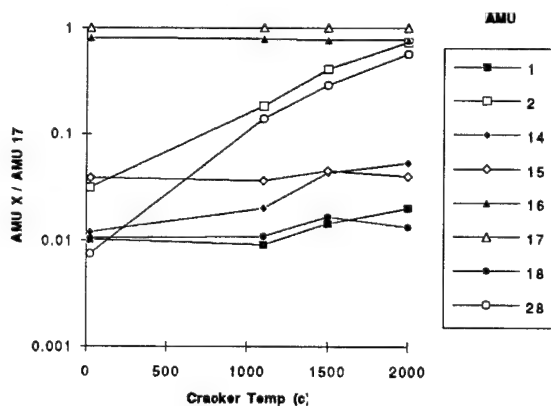Figure 1.   5.00 SCCM NH_3.

Figure 2.   1.00 SCCM NH_3.

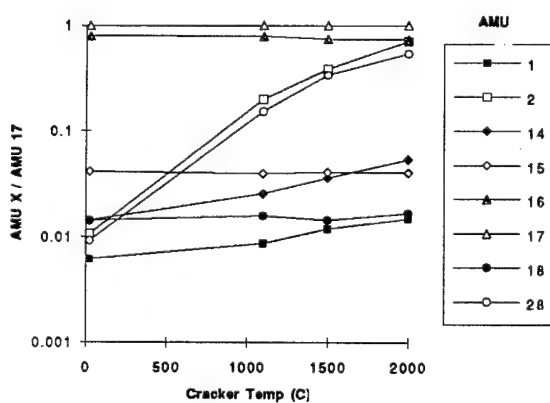Figure 3.   5.00 SCCM NH_3.

Figure 4.   8.00 SCCM NH_3.

20

Analysis of the mass spectrometry data revealed that the cracker cell was cracking the ammonia primarily into molecular hydrogen and nitrogen with very little resulting atomic nitrogen and NH radical species. Since the reactive species are part of the NH_3 cracking pattern in the mass spectrometer itself, providing a detailed discussion on the performance of the cracker cell is difficult. It is surmised that the resulting H_2 and N_2 fluxes are formed from the recombination of NH molecules leaving the surface of the Re filament.

Initial Film Growth. Figures 5-6 show SEM micrographs of GaN deposited directly onto 6H-SiC on-axis wafers provided by Cree Research, Inc. Growth was performed with and without precracking the ammonia in the ammonia cracker. Results reveal that use of the cracker cell to precrack the ammonia leads to a degradation in both film quality and growth rate. By cracking the ammonia directly on the surface of the substrate, a finer and smoother surface morphology is achieved. These results and the results from the RGA data suggest that a reduced growth rate resulting from use of the cracker cell is a consequence of a reduced ammonia flux reaching the substrate, which in-turn provides a reduced supply of NH radicals necessary for film growth.

Figure 5.   GaN (1000A) on 6H-SiC, precracked NH_3 at 1500C, growth temp 800C.
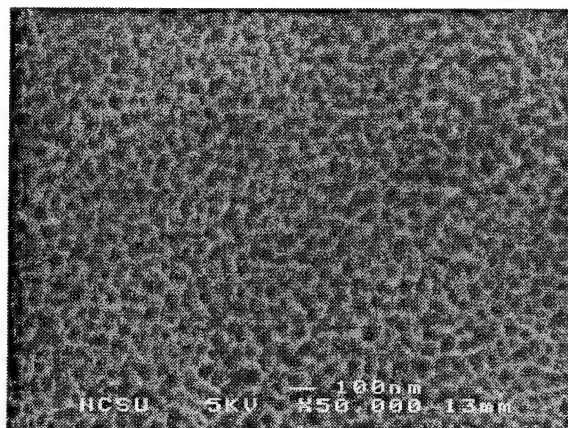
Figure 6.   GaN (3000A) on 6H-SiC, no precracking of NH_3, growth temp 800C.

Although the ammonia cracker did not provide the necessary flux of atomic nitrogen and NH radicals for enhanced film growth, the use of ammonia as a source for the group V species has resulted in a significant improvement in the optical properties of the resulting GaN film. Figure 7 shows the PL spectra taken from a sample grown without the assistance of the ammonia cracker cell. This is the first time this laboratory has produced GaN that has resulted in photoluminence at 354 nm, attributed to the recombination of excitons and neutral donors.

An ECR plasma source was previously used for group V species which proved detrimental to the optical quality of the resulting GaN film.
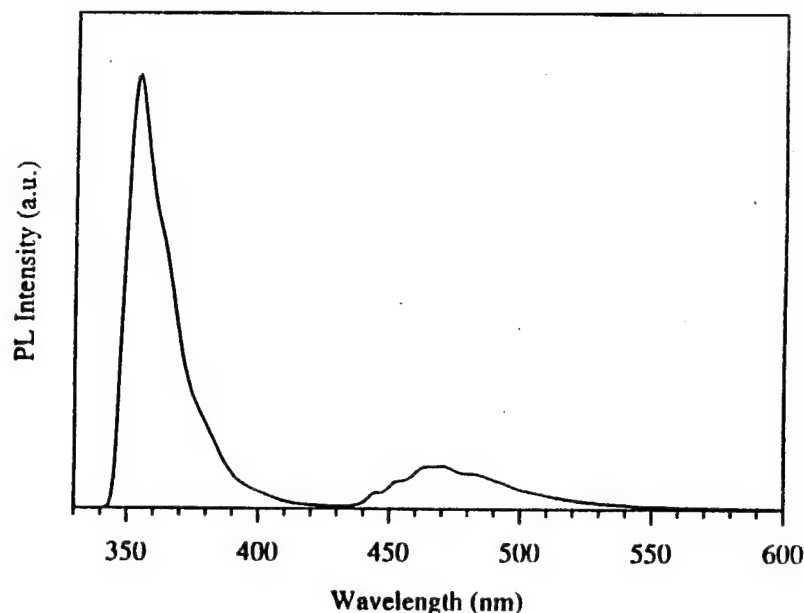
Figure 7.   PL of GaN at 8K.

Figures 8 and 9 show SEM micrographs of AlN grown with and without the assistance of the ammonia cracker. Analysis of these figures reveal that for the case of AlN, no discernible difference occurred in either the morphology or growth rate of the resulting films. However, SIMS analysis of AlN grown using precracked NH_3 indicates Mn impurities have been incorporated into the film at atomic densities as high as 2×10^{20} cm^{-3}. The source of the Mn is thought to be from decomposition of the stainless steel cracker cell sleeve in the vicinity of the heated Rh filament.

Figures 10 and 11 show SEM results of GaN grown on an AlN buffer. These SEM results are typical of the GaN grown to date using AlN buffers without precracked NH_3. As can be seen from Fig. 10, the surface morphology is still considerably rough compared to surfaces obtained by MOCVD growth techniques. However, Fig. 11 shows a drastic reduction in columnar features commonly seen in ECR grown GaN.

D. Conclusions

The use of ammonia (NH_3) thermally cracked on the substrate surface (6H-SiC) has led to a marked improvement in the optical properties of GSMBE grown GaN as characterized by PL spectrum exhibiting a sharp peak at 354 nm in our films for the first time. The use of a high-temperature ammonia-cracking source to precrack the ammonia has resulted in the degradation
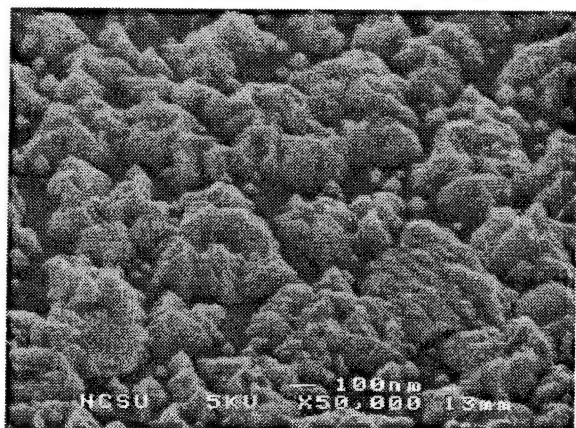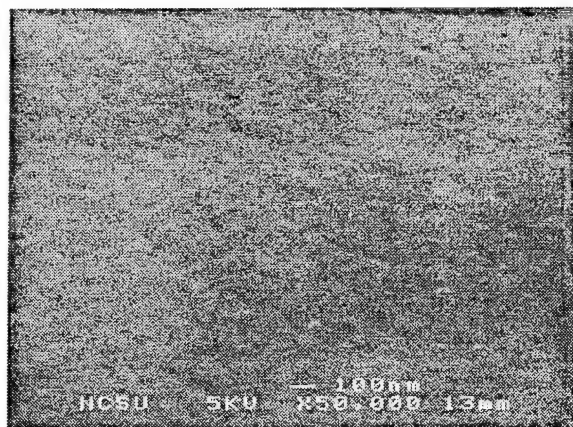
Figure 8.   AlN (3000A) on 6H-SiC, precracked at NH_3 1100C, growth temp 1100C.
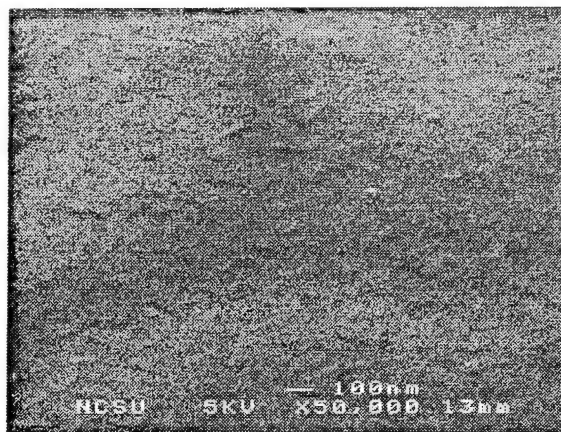
Figure 9.   AlN (3000A) on 6H-SiC, no precracking of NH_3, growth temp 1100C.
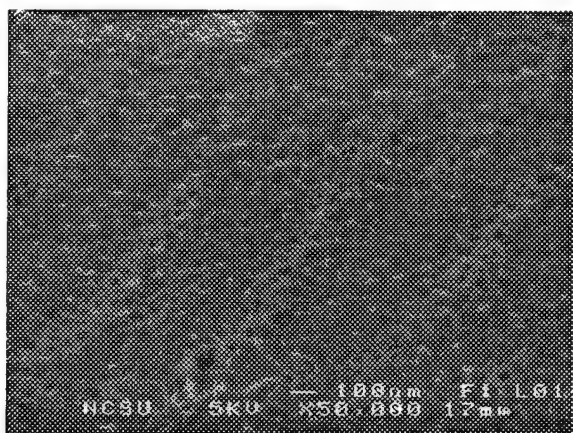
Figure 10.   GaN on AlN buffer.
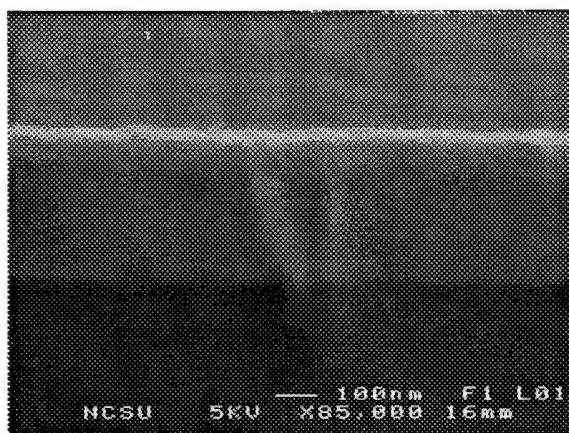
Figure 11.   GaN on AlN buffer.

of both the film morphology and growth rate for GaN. Analysis of RGA spectra reveal that molecular nitrogen and hydrogen are the primary constituents resulting from decomposition of the ammonia. Recombination of NH molecules leaving the Re filament surface are thought to be the source of the N_2 and H_2. This subsequently leads to a reduced growth rate for GaN films.

E.   References

1.   S. Strite, IBM Research Report #83986, March 28, 1994 and private discussions.
2.   J. Smith, D. Chandrasekhar, B. Sverdlov, A. Botchkarev, A. Salvador, and H. Morkoc, Appl. Phys. Lett. **67** (13), 1830 (1995).
3.   W. C. Hughes, *et al.*, J. Vac. Sci. Technol. B **13**(4), 1571 (1995).

4. R. J. Molnar, and T. D. Moustakas, J. Appl. Phys. **76**, (8) 4587 (1994)
5. R. C. Powell, N. E. Lee, Y. W. Kim, and J. E. Greene, J. Appl. Phys. **73**, 189 (1993).
6. M. E. Lin, B. Sverdlov, G. L. Zhou, and H. Morkoc, Appl. Phys. Lett. **62**, 3479 (1993).
7. R. Singh, R. J. Molnar, M. S. Unlu, and T. D. Moustakas, Appl. Phys. Lett. **64**, 336 (1994).
8. W. Hoke, P. Lemonias, and D. Weir, J. Cryst. Growth **111**, 1024 (1991).
9. R. Vaudo, J. Cook, and J. Schetzina, J. Vac. Sci. Technol. B **12**(2) 1232 (1994).
10. W. S. Wong, *et al.*, J. Cryst. Growth, in press.
11 N. Lee, R. Powell, Y. Kim, and J. Green, J. Vac. Sci. Technol. A **13**(5) 2293 (1995).
12. R. C. Powell, N. E. Lee, and J. E. Greene, Appl. Phys. Lett. **60** (20) 2505 (1992).
13. H. Z. Xiao *et al.*, J. Appl. Phys. **76** (12) 8195 (1994).
14. H. Gotoh, T. Suga, H. Suzuki, and M. Kimata, Jpn. J. Appl. Phys. **20**, L545 (1981).
15. S. Yoshida, S. Misawa, and S. Gonda, Appl. Phys. Lett. **42**, 427 (1983).
16. H. U. Baier and W. Mônch, J. Appl. Phys. **68** (2), 586 (1990).
17 H. U. Baier and W. Mônch, J. Vac. Sci. Technol., B **10** (4) 1735 (1992).
18. J. L. Dupuie and E. Gulari, Appl. Phys. Lett. **59**, 549 (1991).
19. J. L. Dupuie and E. Gulari, J. Vac. Sci. Technol. A **10** (1), 18 (1991).
20. G. S. Selwyn and M. C. Lin, Chemical Physics **67**, 213 (1982).
21. Handbook of Chemistry and Physics **73**, 4-24 (1992).
22. S. N. Foner and R. L. Hudson, J. Chem. Phys. **80** (9), 4013 (1984).

V. Luminescence Studies of GaN

A. Introduction

Luminescence is the emission of photons due to excited electrons in the conduction band decaying to their original energy levels in the valance band. The wavelength of the emitted light is directly related to the energy of the transition, by $E=h\nu$. Thus, the energy levels of a semiconductor, including radiative transitions between the conduction band, valance band, and exciton, donor, and acceptor levels, can be measured [1,2]. Various methods exist to excite the electrons, including photoluminescence (photon excitation), and cathodoluminesence (electron-beam excitation). Measurements are often performed at low temperatures (4.2 K using liquid He) to improve luminescence efficiency and distinguish individual transitions.

Both photoluminescence (PL) and cathodoluminescence (CL) analysis have been performed on AlN, GaN, and their solid solutions [3-20]. GaN, with a bandgap of 3.5 eV (354 nm) at 4.2 K, is readily studied by PL using UV sources such as He-Cd and frequency-doubled Ar^+ lasers. This section will focus on GaN; the CL of AlGaN will be discussed in the section devoted to AlGaN growth and characterization.

In the past, GaN grown on vicinal $\alpha(6H)$-SiC(0001)$_{Si}$ wafers has been studied [21]. The PL revealed an intense near band-edge emission at 357.4 nm (3.47 eV), which is attributed to annihilation of excitons bound to neutral donors. The FWHM of this peak, 4 meV, indicated the high quality of the sample. The donor-bound exciton line, often designated the I_2 line, is the signature peak for high quality GaN films. Recently, others have detected free exciton (FE) emission, and evidence of it has been seen in our materials, as well [22-24]. FE emission indicates both the high quality of our materials and a lack of residual donors.

A very weak defect peak ascribed to donor-acceptor pair (DAP) transitions and two associated LO phonon replicas were also discussed previously, with the zero phonon line at 379 nm. Additional structure is found on the low energy side of the 3.27 eV peak at approximately 3.24 eV. Recent work has indicated this structure is due to both DAP transitions and band-acceptor (eA) recombination [25, 26]. This designation has previously been made for transitions at temperatures above 120 K as the thermal energy approaches the shallow donor binding energy. Others believe the additional structure at low temperature is due to a second donor-acceptor pair [27, 28].

Undoped GaN is always n-type, and the origin of the residual donors has been the subject of serious debate. Donors of both extrinsic and intrinsic nature have been proposed. Nitrogen vacancies (V_N) have long been suspected and recent theatrical calculations give credence to this idea [29, 30]. These calculations also suggest that gallium vacancies (V_{GA}) partially compensate n-type GaN. Impurities such as Si and O introduced during growth also increase the carrier concentration and should be minimized.

The identity of the shallow acceptor is unclear, although carbon is a strong possibility [25]. The binding energy of carbon is proposed to be either 200 or 230 meV, depending on whether the transition at 3.27 eV is DAP or eA in nature. The probable source of carbon is the ethyl and methyl radicals used as precursor gases.

B. Experimental Procedures

A combined photo- and cathodoluminesence system is used to measure the luminescence from the III-V nitrides, see Fig 1. Each sample is attached to a cryostat that provides a test temperature range of 4.2 to 300 K. A McPherson model 219 vacuum monochromator with a focusing mirror chamber is used to collect the emitted light. The focal length of the monochromator is .5 m, with a wavelength resolution of .02 nm at 313.1 nm for a 1200 G/mm grating. A photon counting detection scheme is used to measure the light intensity, with a Photomultiplier tube (PMT) that possesses a wavelength range of 180-650 nm.
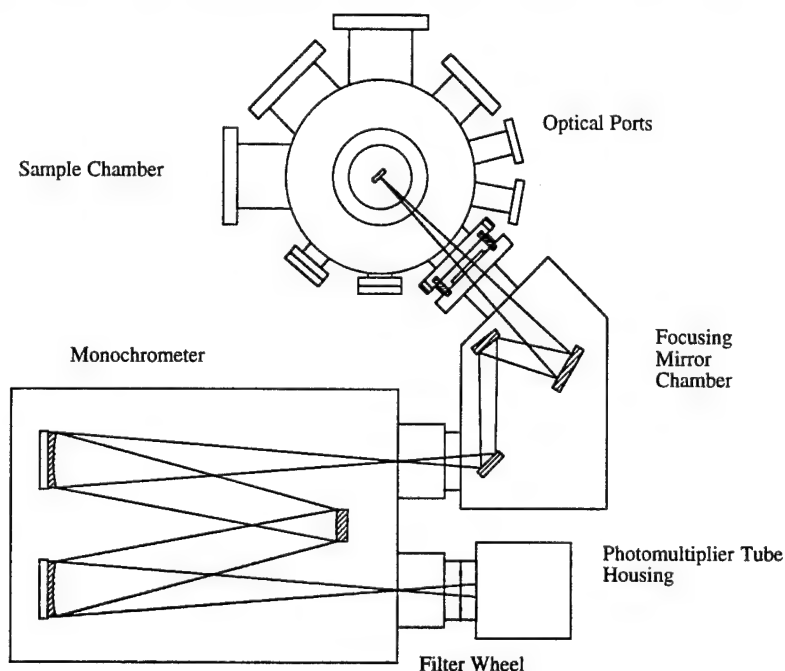
Fig. 1.   Schematic view of combined photo- and cathodoluminescence system.

A Liconix He-Cd laser is the photo-excitation source. It is a continuous wavelength laser that operates at a wavelength of 325 nm (3.8 eV), with a power of 15 mW. It is used for PL of GaN and low $Al_xGa_{1-x}N$ alloys, but a lower wavelength source is required to test the full range of $Al_xGa_{1-x}N$ solid solutions. A Kimball Physics electron gun is used for cathodoluminesence measurements. It has a maximum beam voltage of 10 keV and a maximum beam current of 450 uA. CL experiments are usually performed with a beam voltage of 5 keV and a beam current of 100 uA. A Faraday cup will soon be added to measure the specimen current.

C. Results and Discussion

Photoluminescence measurements were performed on GaN films grown via OMVPE on vicinal and on-axis α(6H)-SiC(0001)$_{Si}$ wafers. The buffer layer for each sample was AlN. All tests were performed at 4.2 K, unless otherwise noted.

In a previous report, both free and bound exciton emission were reported for a 1.4 μm GaN layer deposited on on-axis SiC [22]. The assignment of these peaks has been verified by temperature-dependent PL and the results are shown in Fig. 2. At 4.2 K, the free exciton (FE) peak is at 357.11 nm (3.472 eV) and the bound-exciton (I_2) peak is at 357.79 nm (3.465 eV). As temperature increases, the I_2 intensity decreases much faster than the FE intensity. This behavior is expected and is due to the dissociation of bound excitons as thermal energy (kT) exceeds the binding energy (E_b). Curve fitting performed on the 4.2 K data is displayed in Fig. 3. A Lorentzian energy distribution was assumed for both peaks. The energy difference between the fitted FE and I_2 lines, 7.0 meV, is a measure of E_b. The FWHM of the FE and I_2 lines is 4.86 meV and 4.46 meV, respectively. This is expected, as the bound excitons possess no kinetic energy. Line width is another indication of the identity of both transitions [31].
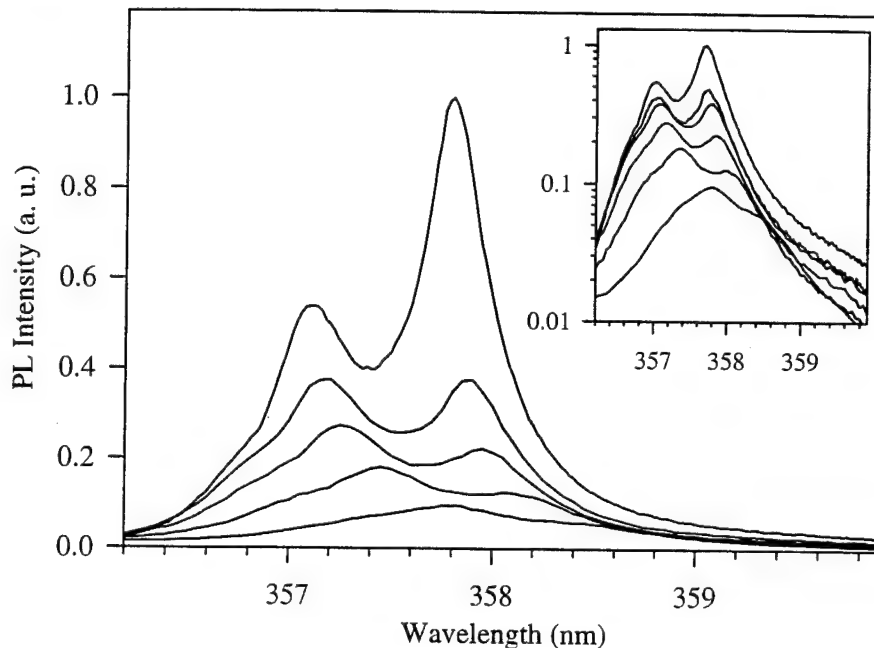
Figure 2.   PL of GaN/on-axis SiC at T=4.2, 25, 35, 50, 70 and 100 K.

In previous work, the PL of GaN at various film thicknesses revealed a shift in the donor-bound exciton peak to lower energies as film thickness increased [22]. This shift was attributed to a change in the bandgap due to strains in the film [31]. A unique sample was used to further study and verify this phenomenon. GaN grown on a whole SiC wafer resulted in a thickness variation of 1.5 μm at the sample center to 1.0 μm at the edge. PL was performed along this

thickness gradient and the results are shown in Fig. 4. These peaks are due to donor-bound excitons, as confirmed by temperature-dependent PL. The energy and wavelength of each peak is displayed in Table I.
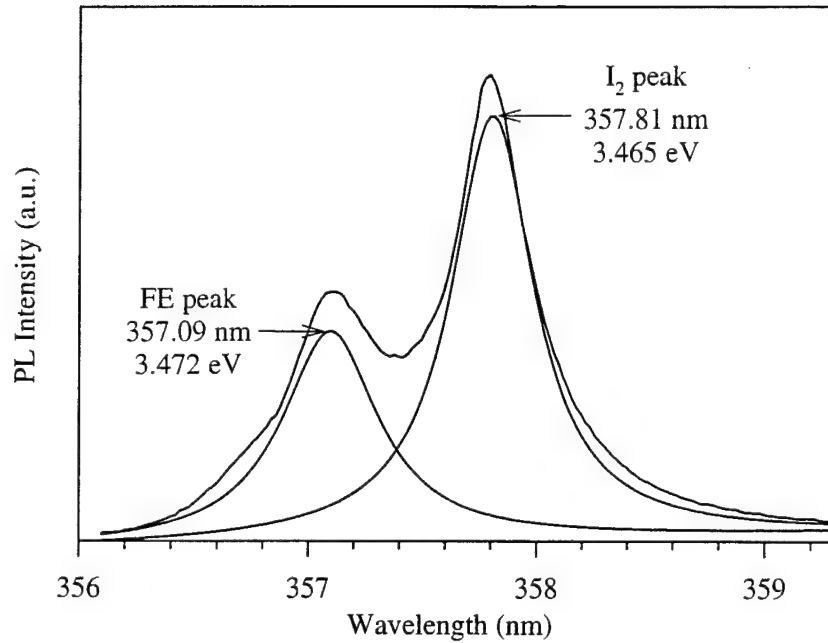
Figure 3.   Curve fitting results for the free exciton (FE) and bound excitor (I₂) PL peaks of GaN on on-axis SiC.
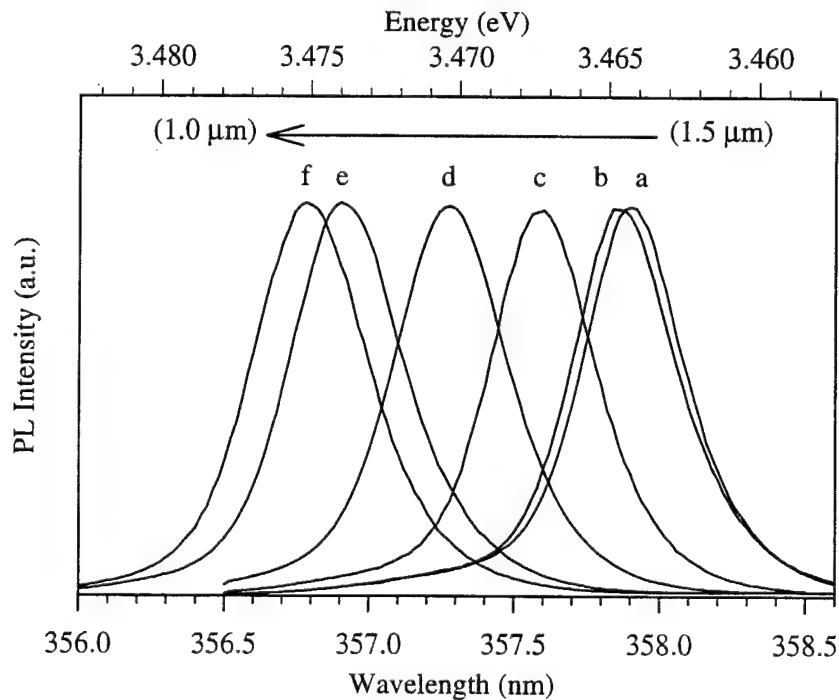
Figure 4.   PL intensity of GaN on SiC at 4.2 K as a function of film thickness.

Table I

Sample	Peak Location (nm)	Peak Location (eV)
a	357.9	3.464
b	357.84	3.465
c	357.6	3.467
d	357.28	3.47
e	356.9	3.474
f	356.78	3.475

The energy shift of 11 meV between peaks a and f is significant, and indicative of a variation in the bandgap of the material due to strain [31].

As film thickness decreases below 1 μm the ratio of DAP to I_2 peak emission intensity increases dramatically. Donor-acceptor pair transition intensity generally increases as the ratio of the number of donors to the number of acceptors (N_D/N_A) approaches unity. Given that undoped GaN is always n-type, an increase in the DAP intensity implies an increase in the number of shallow acceptors. One indication of this is electrical compensation.

Previous work showed the peak ratio for a film grown at 1000°C to be much higher than one at 900°C for the same time period [32]. However, the growth rate also decreased with temperature; the film grown at 900°C was .79 μm and the 1000°C film was .67 μm. Thus, there are two parameters to account for: film thickness and growth temperature. All films were autodoped by precursor impurities and no discernible trend was seen in the electrical data.

After this study, improvements in the growth system have led to higher growth temperatures and better films, with 1050°C the typical growth temperature. Autodoping effects were greatly diminished by changes in the precursor gases. Hence, a similar study was performed for GaN films grown at 950, 1000, 1050 and 1100°C for one hour. The results displayed in Fig. 5 use a log scale for the PL intensity. They confirm that as growth temperature increases (and film thickness decreases), the ratio of the DAP peak intensity to the bound-exciton peak intensity increases. The carrier concentration also decreased with growth temperature and was not able to be measured at the highest growth temperature.

To differentiate between thickness and growth temperature effects, films of equal thickness were grown at 1050 and 1100°C. The PL for both off- and on-axis SiC wafers is displayed in Figs. 6 and 7. The bound exciton and DAP peak intensities are remarkably similar and indicate the decrease in film thickness leads to the intense DAP peaks. The origin of the peak shifts to lower energies for the 1100°C films is unknown. One explanation is that film quality improves with growth temperature, resulting in less mechanisms for strain relief. Further work will be carried out for verification.
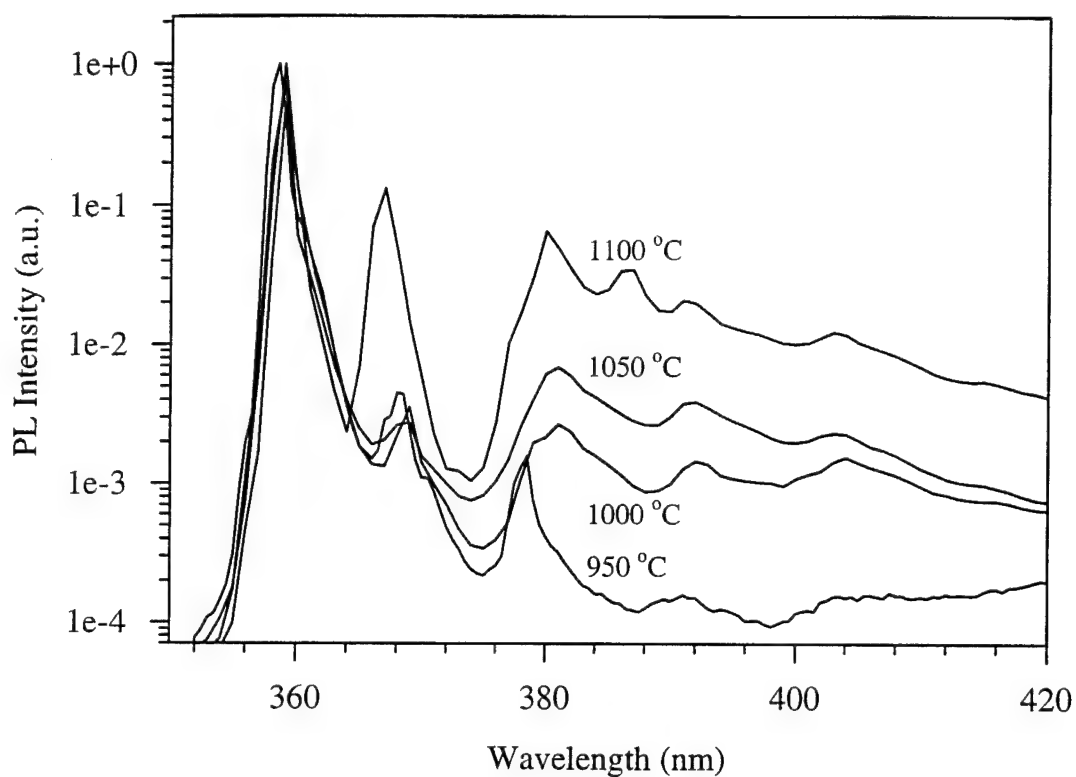
Figure 5.   PL of GaN on SiC at 4.2 K as a function of growth temperature.
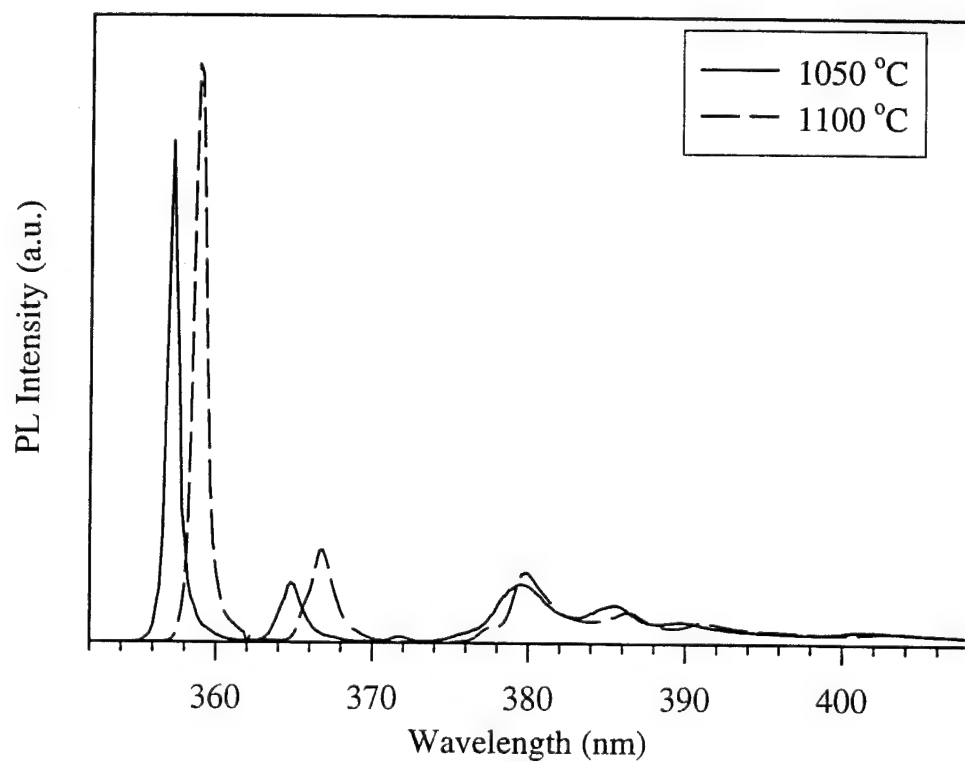
Figure 6.   PL of GaN on off-axis SiC with the same thickness.
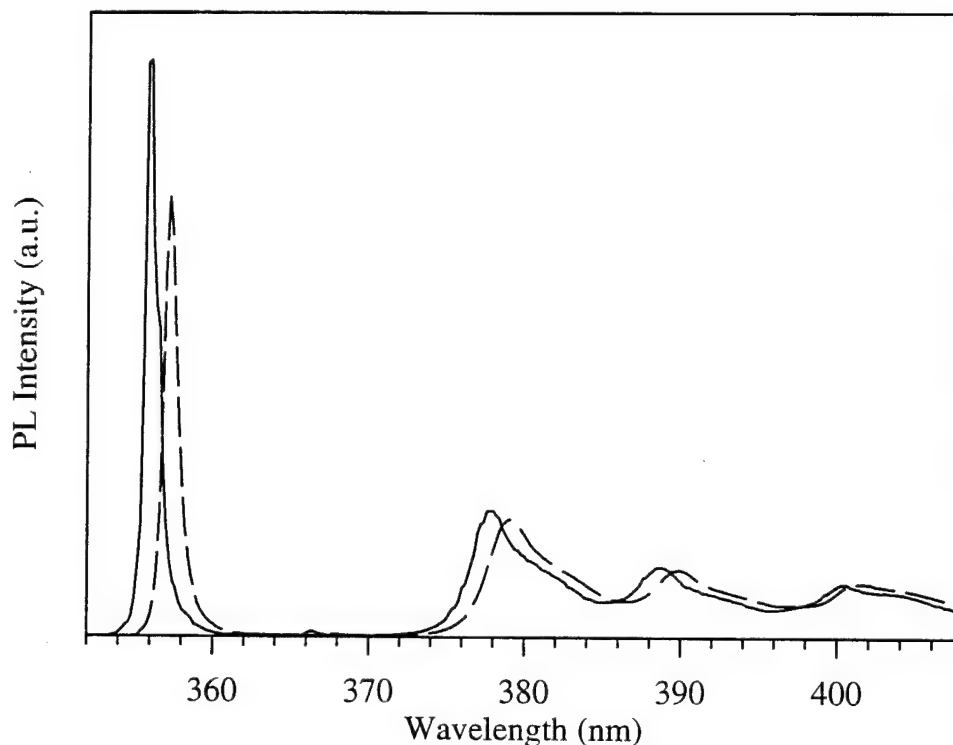
Figure 7.   PL of GaN on on-axis SiC with the same thickness.

These results indicate the increase in DAP peak intensity is due to an increase in N_A near the film/substrate interface. The decrease in film conductivity supports this, as an increase in shallow donors would lead to higher carrier concentrations. Also, n-type doping of GaN by Si shows no increase in DAP peak intensity, while low level p-type doping with Mg does, proof that SAP peaks increase as N_D/N_A approaches unity.

Fischer *et al.* propose carbon as the shallow acceptor, with a binding energy of 230 meV [25]. Carbon has been used successfully as a p-type dopant for GaN grown by MOMBE, although no PL was reported [26]. There are two possible sources of carbon, the SiC wafer and TEG, the gallium source. The SiC wafer is unlikely given the stability of SiC at high temperatures and the presence of the AlN buffer layer. Furthermore, others have similar results for GaN on sapphire. Thus, TEG is the likely source. The high growth temperatures ensure the gallium atoms are detached from the ethyl radicals, eliminating the growth temperature correlation seen typically for GaAs. SIMS profiling of GaN does not indicate higher concentrations of C near the interface, but the variation in concentration required to alter PL may be below the SIMS resolution. In this respect PL is a more sensitive technique.

In related work, Keller *et al.* varied the V/III ratio during growth of GaN. As the V/III ratio decreased, the DAP peak intensity increased. They attribute this to an increase in the nitrogen vacancies (V_N) donors due to a deficiency of active nitrogen species. A preferred explanation is

31

that the V_N are sites for carbon to occupy (C_N), which act as a shallow acceptor. SIMS analysis in a similar study confirms that both the carbon concentration and DAP intensity increases as the V/III decreases [33]. The question, then, is why would there be more vacancies near the film/substrate interface?

One explanation is related to the film microstructure. The majority of threading dislocations ($\sim 1 \times 10^9$ cm^{-2}) are within the first .5 μm for these films and eventually decrease by two orders of magnitude with increasing thickness [21]. It is plausible these dislocations are very efficient at trapping residual donors and acceptors. Given the absorption length of the He-Cd laser is roughly .2 μm in GaN, a noticeable change in the PL spectrum for films .7 μm or thinner should be seen; this is indeed the case.

The threading dislocations form during film growth due to the lattice mismatch between GaN and SiC (3.4 %). It is possible that carbon and other species could segregate to the dislocation core along the surface or at a later time at the growth temperature. In general point defects such as impurities and vacancies segregate to dislocations to reduce their strain energy with the lattice.

Recent work Sverdlov *et al.* supports this explanation [34]. They propose the vertical defects observed in GaN are stacking mismatch boundaries (SMBs), which are boundaries between differently stacked domains originating at the SiC substrate steps. The lattice is severely distorted at these boundaries, which can be interpreted as a two-dimensional network of quasinterstial atoms or quasivacancies. This network may act as an effective sink for introduced impurities. Carbon is a very small atom and so it is reasonable large amounts could pile up at these defects and act as shallow acceptors.

Electron spin resonance (ESR) and Hall-Vander Pauw measurements by Carlos *et al.* showed strong evidence of compensation near the film/substrate interface for GaN on sapphire using an AlN buffer layer [35]. They attributed this to an increase in shallow acceptors near the interface, possibly due to the aforementioned dislocations. A similar trend for a GaN buffer layer did not occur, however, indicating the AlN buffer layer used for our materials may be a source of compensating acceptors.

The arrows in Figs. 8 and 9 point out additional peaks unusual for GaN. They are most intense in two samples grown at 1100°C, but they also present (albeit weaker) in Figs. 6 and 7. The peak at 365.8-366.2 may be due to an acceptor-bound exciton (I_1), although no report of a bound exciton at such a low energy exists. The peaks at 385.1-.4 appear to be a second donor-acceptor pair. Given that the sample appears to be compensated, it is believed this is due to a second acceptor level, possibly one that gives the I_3 peak noted above. There is no indication of additional impurities introduced into these samples.
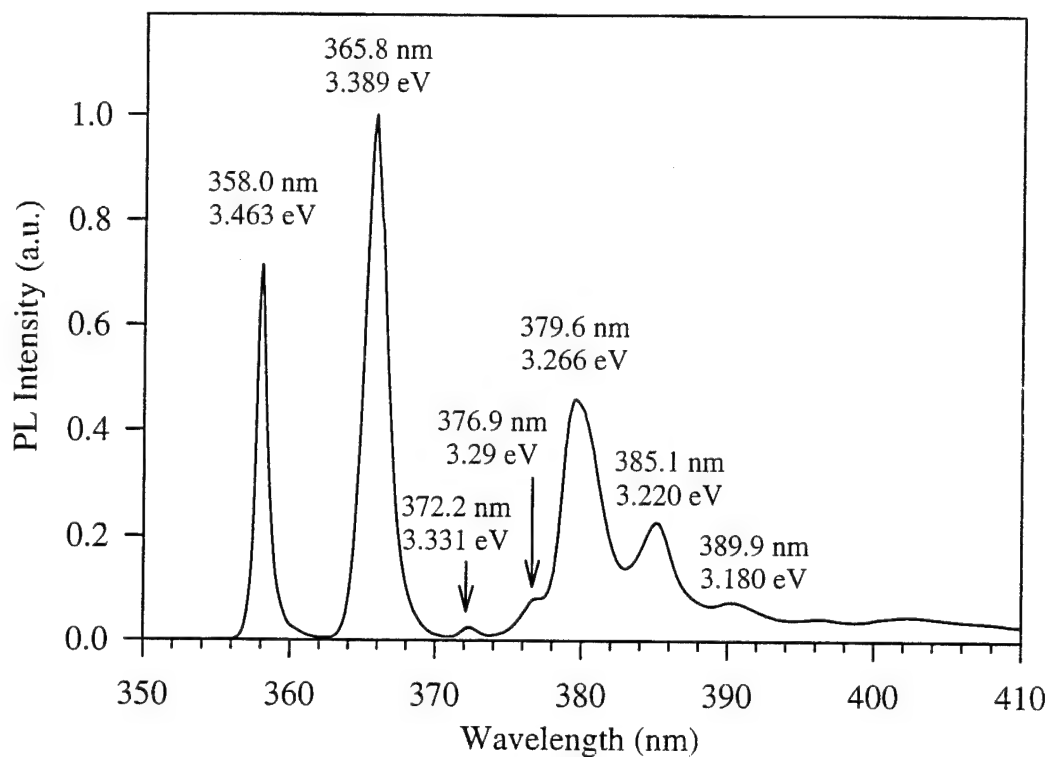
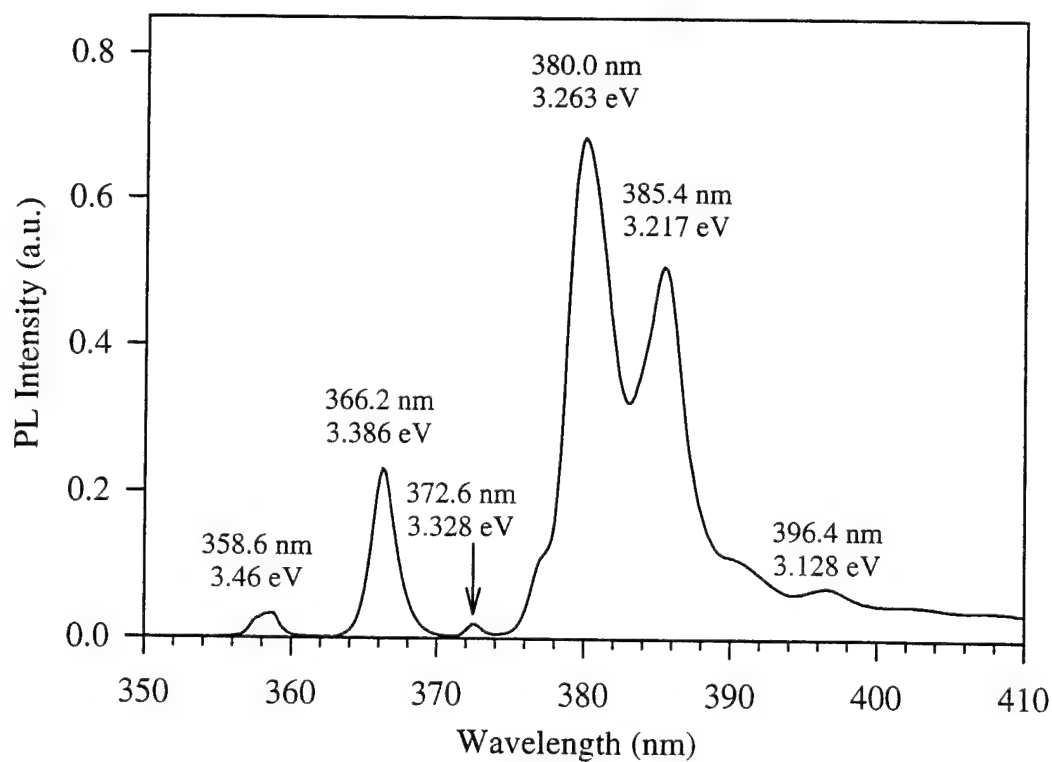Figure 8.   PL of GaN on on-axis SiC at 1100°C.

Figure 9.   PL of GaN on off-axis SiC at 1100°C.

D. Conclusions

Temperature dependent PL was used to verify free exciton emission for GaN on SiC. Curve fitting showed the binding energy of the excitons to neutral donors to be 7 meV. The smaller FWHM of the free exciton peak is further confirmation of it's nature.

An 11 meV shift in the I_2 line was observed for a GaN film with a .5 μm thickness variation. This shift is considerable and results from a variation in the bandgap energy due to strain effects.

The ratio of DAP to I_2 peak emission intensity increased dramatically as film thickness decreased below .8 μm. This behavior is attributed to an increase in shallow acceptors near the film interface, with carbon the likely acceptor. We believe the high density of threading dislocations (SMBs) act as traps for carbon, either at interstitial and/or vacancy sites.

E. References

1. B. G. Yacobi and D. B. Holt, *Cathodoluminescence Microscopy of Inorganic Solids*, Plenum Press, New York (1990).
2. M. D. Lumb, Ed., *Luminescence Scpectroscopy*, Academic Press, New York (1978).
3. S. Strite and H. Morkoç, J. Vac. Sci. Technol. B **10** (4), 1237 (1992).
4. R. A. Youngman and J. H. Harris, J. Am. Ceram. Soc. **73** [11], 3238 (1990).
5. S. Nakamura, T. Mukai, and M. Senoh, Jpn. J. Appl. Phys. **30** (10A), 1708 (1991).
6. V. F. Veselov, A. V. Dobrynin, G. A. Naida, P. A. Pundur, E. A. Slotensietse, and E. B. Sokolov, Inorganic Materials **25** (9), 1250 (1989).
7. J. N. Kuznia, M. A. Kahn, D. T. Olson, R. Haplan, and J. Freitas, J. Appl. Phys. **73** (9), 4700 (1993).
8. H. Murakami, T. Asahi, H. Amano, K. Hiramatsu, N. Sawaki, and I. Akasaki, J. Crystal Growth **115**, 648 (1991).
9. K. Maier, J. Schneider, I. Akasaki, and H. Amano, Jpn. J. Appl. Phys. **32** (6), 846 (1993).
10. I. Akasaki, and H. Amano, J. Crystal Growth **99**, 375 (1990).
11. S. Yoshida, H. Okumura, S. Misawa, and E. Sakuma, Surf. Sci. **267** (7), 50 (1992).
12. S. Nakamura, T. Mukai, and M. Senoh, Jpn. J. Appl. Phys. **31** (9), 2883 (1992).
13. S. Nakamura, N. Iwasa, T. Mukai, and M. Senoh, Jpn. J. Appl. Phys. **31** (5), 107 (1992).
14. S. Nakamura, T. Mukai, and M. Senoh, Jpn. J. Appl. Phys. **30** (12A), 1998 (1991).
15. S. Strite, J. Ruan, Z. Li, N Manning, A. Salvador, H. Chen, D. J. Smith, W. J. Choyke, and H. Morkoç, J. Va. Sci. Technol. B **9** (4), 1924 (1991).
16. W. J. Choyke and I. Linkov, Inst. Phys. Conf. Ser. **137**, 141 (1993).
17. S. Pacesova and L. Jastrabik, 1979 Phys. Stat. Sol. B **93**, K111.
18. S. Yoshida, S. Misowa, Y. Fujii, S. Takada, H. Hayakawa, S. Gonda, A. and Itoh, J. Vac. Sci. Technol. **16** (4), 990 (1979).
19. E. R. Glaser, T. A. Kennedy, H. C. Crookham, J. A. Freitas, Jr., M. Asif Khan, D. T. Olson, and J. N. Kuznia, Appl. Phys. Lett. **63** (19), 2673 (1993).
20. E. R. Glaser, in *Proceedings of the 18th International Conference on Defects in Semiconductors*, to be published.
21. T. W. Weeks, Jr., M. D. Bremser, K. S. Ailey, E. Carlson, W. H. Perry and R. F. Davis, Appl. Phys. Lett. **67** (3) 17, (1995).
22. R. F. Davis, M. D. Bremser, K. Gruss, K. Linthicum, B. Perry. and T. W. Weeks, Jr., Semiannual Technical Report for ONR Grant #N00014-92-J-1720, June 1995.

23. W. Shan, T. J. Schmidt, X. H. Wang, S. J. Hwang, J. J. Song, and B. Goldenbergm Appl. Phys. Lett. **66**, 985 (1995).
24. D. Volm, T. Strebl, B. K. Meyer, T. Detchprohm, H. Amano, and I Akasaki, Sol. St. Comm. **96** (2), 53 (1995).
25. S. Fischer, C. Wetzel, E. E. Haller, and B. K. Meyer, Appl. Phys. Lett. 67 (9), 1289 (1995).
26. C. R. Abernathy, J. D. MacKenzie, S. J. Pearton, and W. S. Hobson, Appl. Phys. Lett. **66** (15), 1969 (1995).
27. R. Dingle and M. Ilegems, Solid State Commun. **9**, 175 (1971).
28. E. R. Glaser, T. A. Kennedy, S. W. Brown, J. A. Freitas, Jr., W. G. Perry, M. D. Bremser, T. W. Weeks, and R. F. Davis, to be published.
29. P. Boguslawski, E. L. Briggs, and J. Bernholc, Phys. Rev B. **51** (17), 255 (1995).
30. J. Neugebauer and C. G. Vad de Walle, Phys. Rev. B **50**, 8067 (1994).
31. J. I. Pankove, *Optical Processes in Semiconductors*, Dover, New York (1971).
32. R. F. Davis, M. D. Bremser, K. Gruss, K. Linthicum, B. Perry. and T. W. Weeks, Jr., Semiannual Technical Report for ONR Grant #N00014-92-J-1720, December 1994.
33. A. Ishibashi, H. Takeishi, M. Mannoh, Y. Yabuuchi, and Y. Ban, to be published.
34. B. N. Sverdlov, G. A. Martin, H. Morkoc and D. J. Smith. Appl. Phys. Lett. **67** (14), 2063 (1995).
35. W. E. Carlos, J. A. Freitas, Jr., M. A. Khan, D. T. Olson, and J. N. Kuznia, Phys. Rev. B. **48** (24), 17878 (1993).

VI. Surface Cleaning and Contact Formation on n-type and p-type GaN

A. Introduction

The formation of ohmic contacts with semiconductor materials and devices is a fundamental component of solid state device architecture. As device size has diminished and the scale of integration has increased, the quality of these interfaces has become an increasingly important concern. In addition, the presence of parasitic resistances and capacitances, such as those existing at contact interfaces, becomes more detrimental at higher operating powers and higher oscillation frequencies. For many devices, the losses that occur at the contact interfaces account for a large fraction of the total losses and, as such, are responsible for significant impact on device performance.

The development of adequate and reliable ohmic contacts to the compound semiconductors, particularly those with wider bandgaps, has met a number of challenges. The subject of ohmic contacts to p- and n-type III-V compounds, mostly GaAs, AlGaAs, and InP, has received a great deal of attention over the past decade and significant advances have been made [1-12]. By comparison, the III-V nitrides have received little attention in this regard. However, interest in these materials has been renewed in recent years as great strides have been made in the successful, commercial implementation of bright blue GaN LED devices.

GaN Surface Cleaning. Over the course of the development of semiconductor device technology, surface cleaning procedures have been devised to 1) degrease and remove gross contamination, 2) remove particulates and metal atom contamination, and 3) remove surface oxides to provide surfaces as atomically clean as possible. In practice, surface cleaning is as much of an art form or craft as it is a science; understanding of the surface composition and structure often lags well behind the successful application of processing steps. Procedures are frequently derived empirically with little detailed understanding of the chemistry or physics involved. Often, the meaning of the word "clean" varies depending on the surface conditions required for success with different processing steps, though surface impurity concentrations may vary by orders of magnitude. Given that the sensitivity of surface analytical techniques for detection of submonolayer coverage is limited, there are inherent limits on the ability to show conclusively that a surface is truly atomically clean [13].

As stated above, there are indications in the literature that cleanliness and preparation of the semiconductor surface prior to contact deposition play significant role in the performance of the interface. The goal of the surface cleaning studies described in this report is to determine the most effective choices of wet chemical cleaning and thermal desorption cleaning to use prior to metallization.

36

Metallization Strategies. The majority of successful ohmic contact systems that have so far been implemented with the more conventional compound semiconductors have relied upon alloying (liquid-phase reaction) or sintering (solid-phase reaction) via post-deposition annealing treatments, and/or the presence of high carrier concentrations near the interface [1,2,6,12]. However, many otherwise successful ohmic contact systems have only limited thermal stability and are subject to degradation—usually in the form of extensive interdiffusion, interfacial reaction, and interphase growth, accompanied by increase in contact resistivity—under subsequent thermal processing steps. It is reasonable to suppose that the cleanliness and preparation of the semiconductor surface prior to contact deposition plays a significant role in the behavior of the interface, and there are indications in the recent literature that support this [2,11,12,14]. Thorough oxide removal is especially important, though it may well prove to be a persistent challenge with Al-containing compounds in particular.

In this study, two main approaches are being taken in the development of ohmic contacts to GaN and AlN. The first approach is similar to that which has resulted in the majority of successful ohmic contacts to the more conventional compound semiconductors such as GaAs: the creation of high carrier concentrations in the semiconductor at the metal interface by means of alloying, sintering, or implantation of dopant species. The so-called pinning of the Fermi level at this surface, particularly with GaAs, results in a more or less fixed potential barrier at the metal interface. In the case of the pinned Fermi level of GaAs, the approach has generally been to shrink the width of the depletion layer by means of increasing the carrier concentration to the point where carriers tunnel readily through the barrier. Even with optimization of contact composition and annealing times and temperatures, the lowest contact resistivities (ρ_c) have been obtained only on the most heavily doped materials. Though there are indications that high doping levels and extensive interfacial reactions through alloying and sintering are not essential for ohmic contact formation in all cases, these processes have proven useful for minimizing ρ_c [2,11,12,14].

The other approach toward ohmic contact formation to be taken in this study involves the Schottky-Mott-Bardeen (SMB) model of semiconductor interfaces [15,16]. In this model the relative values of work function of the materials involved determine the band structure of the interface and thus the nature of any potential barriers present. The presence of interfacial states at the semiconductor surface can interfere with the alignment of the Fermi level across the interface and overshadow the effect of the inherent difference in work function between the two materials. The III-V nitride compounds are more ionically bonded than their phosphide and arsenide counterparts, as a result of larger electronegativity differences between the component elements. According to the observations of Kurtin *et al.* [17], this fact indicates that the nitrides should experience less Fermi level stabilization or "pinning" at the surface than do the more covalent compounds. Thus, the barrier heights of contacts to the nitrides should be more

37

dependent on the contact material than is the case with the more conventional and more covalent semiconductors such as Si, GaAs, InP, SiC, etc. With the work of Foresi and Moustakas [18,19], M.E. Lin *et al.* [20], Binari *et al.* [21], and the present authors, investigation of this concept is now underway. The SMB model also indicates that the cleanliness of the interface plays an important role in its electrical behavior, particularly in the minimization or elimination of any insulating layers at the interface.

One area of contacts development that has received a significant amount of attention is that of the metal silicide compounds. Silicide thin films have been extensively studied and applied as contacts and interconnects, mostly for silicon-based technology [22-27]. In comparison, the properties of the metal germanides are not well documented. As a general rule, germanides have been found to be more resistive than silicides and their chemistry with Si-based materials more complex. However, in a series of studies, M. O. Aboelfotoh *et al.* have shown that a particular phase of copper germanide, specifically the ordered monoclinic phase ε_1-Cu_3Ge, is an exception to these rules [28-31]. Thin films of Cu_3Ge exhibit remarkably low resistivities, unlike Cu_3Si and, unlike both Cu and Cu_3Si, are surprisingly stable with respect to oxygen and air exposure. As such, Cu_3Ge presents itself as a potentially useful contact metal. Indeed, preliminary experimentation with Cu_3Ge contacts on GaAs and GaN, primarily on n-type and heavily-doped p-type material, has produced some favorable results in terms of ohmic contact formation. For these reasons, copper-germanium contacts were investigated during this reporting period as possible candidates for high-quality, low-resistivity ohmic contacts.

B. Experimental Procedure

GaN Film Deposition. The substrates used for III-nitride film growth were 6H-SiC wafers supplied by Cree Research, Inc. The III-N films used in these contacts studies were grown by means of metalorganic vapor phase epitaxy (MOVPE). The growth reactor used for the nitride film deposition is described in other sections of this report. Magnesium incorporated into the films during growth as the p-type dopant, Ge, was used to grow n-type material via MBE and Si was used as the more effective donor impurity for the MOVPE-grown films.

Surface Analysis. Auger electron spectroscopy (AES) was used to characterize the presence of chemical impurities on the cleaned GaN surfaces. This technique involves the energy analysis of characteristic electron emission from the surface of a sample in response to an incident electron beam. Like the related technique x-ray photoelectron spectroscopy (XPS), which uses incident x-ray radiation as the primary energy source, AES allows the detection of atoms in the first few atomic layers of a surface (1-5 nm) to a sensitivity of approximately 0.5-1%. This sensitivity corresponds under most conditions to submonolayer coverage and thus, is usefully applied to studying the contamination of surfaces by oxide and hydrocarbon deposition.

Auger electron spectroscopy was performed at the NCSU Surface Science Laboratory, using an AES analysis system manufactured by VG Instruments Ltd. Incident beam energy was 3 kV with a spot size of 1 m. Spectra were acquired over the energy range 30-1230 eV, with an energy resolution of 1 eV/step.

Contact Deposition. Prior to metals deposition, the GaN/SiC films were cleaned with a 1:1 HCl:DI H_2O dip and carefully pulled dry from the solution. Any remaining cleaning solution was blown dry with N_2. The UHV system used for the Ti, TiN, and Cu_3Ge depositions provided the means for heating the samples in vacuum. In these cases, the GaN samples were thermally desorbed at 700°C for 15 min for further cleaning of the surfaces. Titanium and TiN were grown on Si-doped GaN (MOVPE-grown, n=1.2×10^{18} cm^{-3} and n=7.4×10^{18} cm^{-3}) using electron beam evaporation of Ti; for TiN deposition, purified N_2 activated by a Kaufman-type ion gun was added. Both the Ti and TiN growth were performed at a substrate temperature of 350°C and a deposition rate of 10-15 Å/min. Total thickness for both metal films was 1000 Å. Auger depth-profiling analysis of TiN films grown under these conditions have revealed them to be stoichiometric TiN and uniform through the thickness even when variations in pressure and deposition rate occurred during growth. In addition, the metallic gold-like appearance of the TiN compound is a reliable indicator of stoichiometry. Film thicknesses were monitored using a quartz crystal oscillator. The Cu_3Ge contacts on n-type GaN (MOVPE, Si-doped) were deposited at NCSU in a UHV electron beam evaporation system. The Cu and Ge components of this contact system were deposited sequentially, 800 Å layers of Cu followed by 1200 Å of Ge; these film thicknesses place Cu and Ge on the GaN surface with a Cu:Ge atomic ratio of 3:1. The alloying of the layers was accomplished by heating at 400°C for 15 minutes while in vacuum after the metal evaporation, as described by Aboelfotoh *et al.* [27-30]. The TLM patterns for the Ti, TiN, and Cu_3Ge contacts were defined using photolithography. On p-GaN:Mg, Pt films were deposited by means of Ar ion sputtering using a shadow mask to define the test pattern. No thickness monitor was available in the sputtering system; but from the sputter time, voltage, and current, the deposition was expected to result in a film approximately 600 Å thick.

Contact Characterization. After deposition, I-V measurements were taken between separate pads of the TLM patterns using tungsten probe tips and an HP 4145C Semiconductor Parameter Analyzer. Annealing treatments for the Ti, TiN, and Pt contacts were performed in a flowing Ar atmosphere (ultra-pure carrier grade from Air Products, Inc.) at a series of temperatures (600, 700, 800 and 900°C for 30 s each step) using a Heatpulse 410 rapid thermal annealing (RTA) furnace. The Cu_3Ge contacts were annealed under UHV conditions at 600, 700, and 800°C for 15 min at each step. TLM measurements were taken by measuring the total resistance between identical contact pads as a function of separation distance 1. The contact resistivity was obtained from the plot of R(1) vs. 1, as described by Reeves and Harrison [32].

The mathematical assumptions and pattern geometry inherent in this model yield values for ρ_c that represent an upper limit; thus, the measured values are conservative assessments of performance. In addition, for every test pattern geometry there is a lower limit of ρ_c below which it is not possible to obtain precise ρ_c calculations. This is due to the fact that the linear R(l) plot becomes very steep and too close to the origin with decreasing ρ_c. For the shadow-mask test geometry used in this study to date and for many of the TLM results reported by other researchers in the field, the practical lower limit for precise ρ_c calculation is about 10^{-6} $\Omega \cdot cm^2$.

C. Results

GaN Surface Cleaning. Acquired AES spectra from surfaces cleaned in a variety of wet chemical solutions are shown in Fig. 1. The label "DI" refers to deionized water; the term "solvent cleaning" refers to the conventional sequence trichloroethylene (TCE), acetone, and methanol (MeOH); all of the samples were solvent-cleaned prior to the acid dip step. The last cleaning step for each sample was followed by blowing dry with N_2, without water rinse. The as-received sample was exposed to air for at least a week prior to characterization; all of the cleaned samples were loaded into the vacuum system (base pressure 5×10^{-9} T and below) as soon as possible. Each received an unavoidable exposure to air for approximately 10 minutes during the time required to secure each sample to the sample holder.

For the purpose of graphing these data, the nitrogen peak-to-peak heights were all set to the same value so that the relative concentrations of O and C may be compared. The associated data of peak height ratios are listed in Table I. The peak-to-peak heights of the oxygen and carbon signals are related to the peak-to-peak height of the nitrogen signal and indicate the relative abundance of oxygen-based and carbon-based surface coverages. The ratios of peak heights have been used because, though the total number of counts in a given peak may vary from run to run, the *relative* peak intensities remain the same for a given surface.

Table I. Relative Auger Peak Intensities from GaN Surfaces Cleaned
with Different Wet Chemical Treatments

Treatment	O/N	C/N
As-received	0.39	0.28
UV/ozone oxidized	0.98	0.31
HCl:DI (1:1)	0.21	0.24
HCl:MeOH (1:1)	0.24	0.32
HF:DI (1:20)	0.33	0.38
HF:DI (1:1)	0.26	0.18
HF:MeOH (1:1)	0.33	0.41
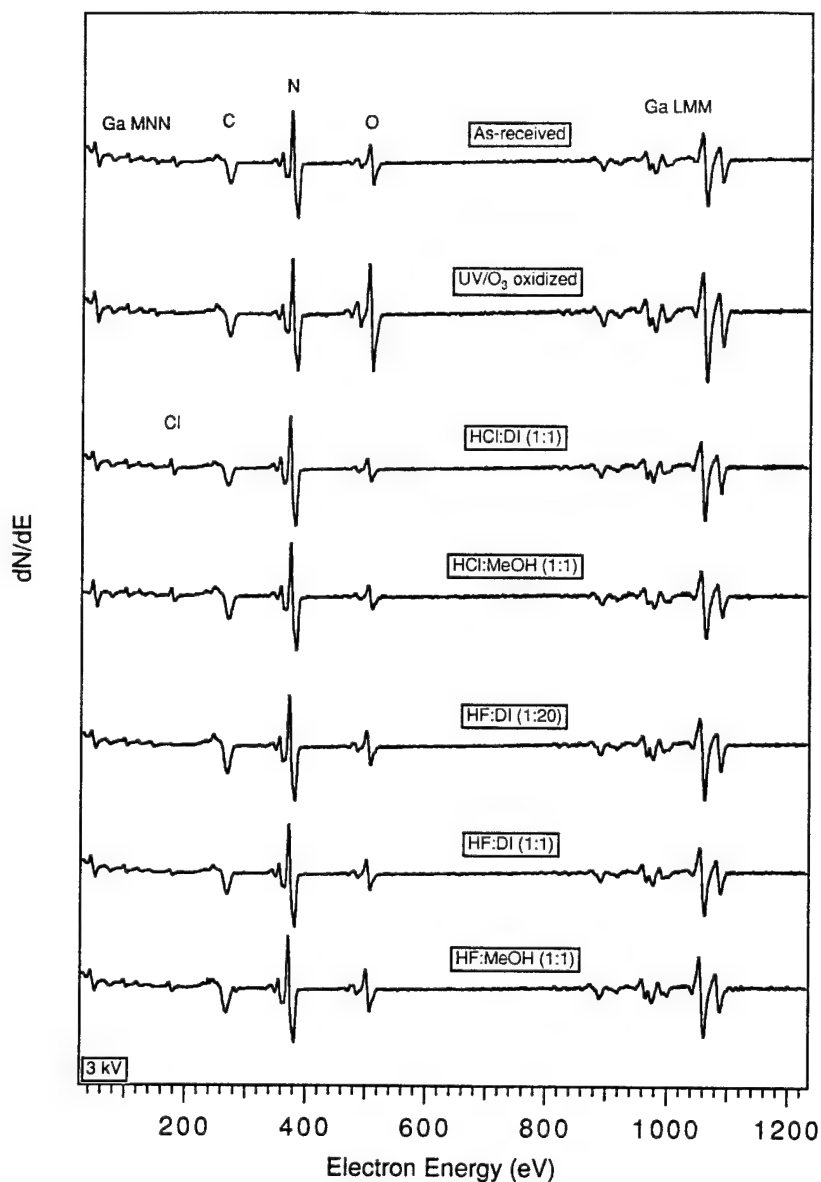
Figure 1.   AES survey spectra of GaN surfaces cleaned with different chemical treatments.

Of all the wet chemical cleaning methods compared here, the HCl:DI (1:1) solution yielded the lowest relative concentration of oxygen on the air-exposed surfaces. A substantial decrease in O coverage after HCl- and HF-based cleaning treatments has been observed for both simple air-exposed and UV/ozone oxidized GaN surfaces indicating the actual removal of surface oxides. The use of methanol to dilute the HCl solution resulted in an increase of both O and C, presumably due to the physisorption of methanol, though both HCl-based solutions resulted in lower O/N ratios than did any other surface condition examined. All of the remaining cleaning treatments showed larger relative concentrations of both O and C, with the exception of HF:DI producing an as-cleaned C/N ratio of 0.18. Of all the HF cleaning treatments examined, the

HF:DI (1:1) treatment gave the lowest O and C concentrations. The highest concentrations of O and C observed were found on the HF:MeOH-treated surface, slightly higher than those on the as-received surface.

The effects of heating GaN surfaces on the presence of O and C are shown in Fig. 2. The following HCl-based and HF-based cleaning methods were compared: HCl:DI (1:1), HCl:MeOH (1:1), HF:DI(1:1), and HF:MeOH (1:1). All of the desorption series show a gradual decrease in the presence of O and C through 650°C. However, small but detectable amounts of O and C were still present on the GaN surfaces even after heating to 800°C. During the 800°C heating steps, residual gas analysis in the UHV heating chamber revealed the presence of small amounts of gas-phase Ga released by the samples, indicating the beginnings of GaN decomposition. The relative proportions of O and C that remained on each surface after the desorption series were different for the HCl-cleaned and HF-cleaned samples: after the 800°C desorption step, the HCl-cleaned surfaces showed the lowest O levels, while the HF-cleaned surfaces showed the lowest C levels.

Table II. Relative AES Peak Intensities for GaN Surfaces as a Function of Temperature and Surface Treatment.

Desorption Temperature	HCl:DI (1:1)		HCl:MeOH (1:1)		HF:DI (1:1)		HF:MeOH (1:1)	
	O/N	C/N	O/N	C/N	O/N	C/N	O/N	C/N
RT	0.21	0.24	0.23	0.31	0.26	0.18	0.41	0.33
500°C	0.18	0.17	0.16	0.27	0.16	0.16	0.18	0.32
625°C	0.14	0.14	0.16	0.25	0.17	0.13	0.16	0.24
800°C	0.39	0.17	0.15	0.21	0.19	0.08	0.17	0.29

Ti and TiN Contacts on n-GaN:Si. The as-deposited Ti contacts on Si-doped, MOVPE-grown n-GaN exhibited rectifying behavior and high resistance. The TiN contacts were deposited on GaN of two different carrier concentrations ($n=1.2\times10^{18}$ cm^{-3} and $n=7.4\times10^{18}$ cm^{-3}); in both cases the TiN contacts were ohmic in the as-deposited condition, though the higher-doped samples showed substantially lower resistance in current-voltage measurements. For the lower-doped n-GaN, TLM measurements of TiN/n-GaN yielded as-deposited ρ_c values of 650 $\Omega\cdot$cm^2. The specific contact resistivities and high series resistance in the as-deposited Ti/n-GaN and TiN/n-GaN ($n=1.2\times10^{18}$ cm^{-3}) contacts decreased sharply in response to annealing, as shown in Figs. 3 and 4, respectively. After the 600°C
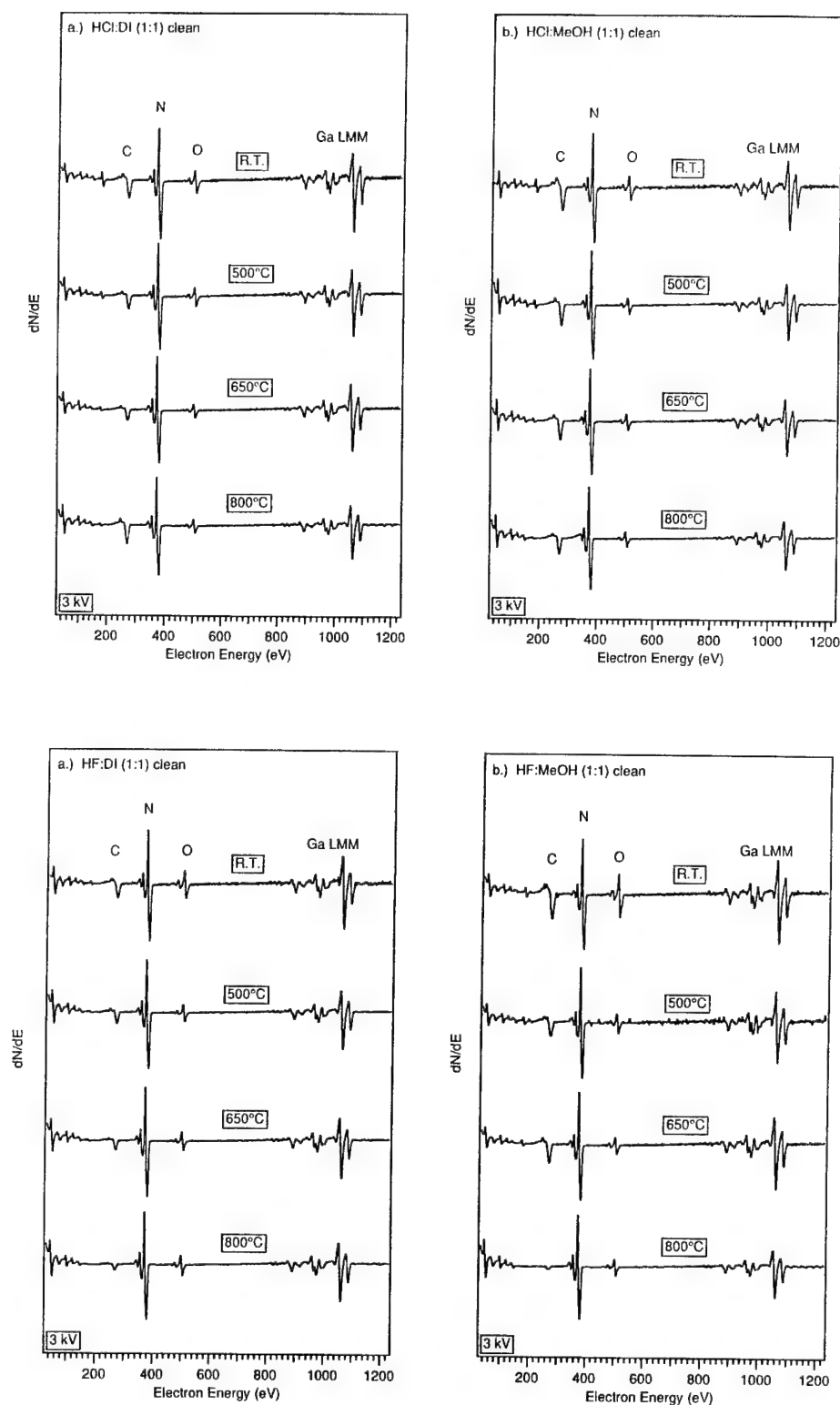
Figure 2.   AES survey spectra of GaN surfaces as a function of temperature.

anneal, the Ti contacts lost most of their rectifying character and the overall resistance decreased markedly. With subsequent anneal steps through 900°C, the ρ_c of both contacts dropped substantially; the TiN contacts reached 1.1×10^{-2} $\Omega\cdot cm^2$ and the Ti contacts reached

Figure 3.   Evolution of I-V behavior for (a) Ti and (b) TiN metal contacts on n-GaN as a
function of annealing temperature.

Figure 4.   Specific contact resistivity ρ_c for Ti and TiN contacts on n-GaN ($n=1.2\times10^{18}$ cm^{-3}) as a function of annealing temperature.

9.9×10^{-3} $\Omega\cdot$cm^2. The TiN contacts on the more highly doped GaN ($n= 7.4\times10^{18}$ cm^{-3}) exhibited low-ρ_c behavior is the as-deposited condition; TLM measurements revealed a low room temperature specific contact resistivity o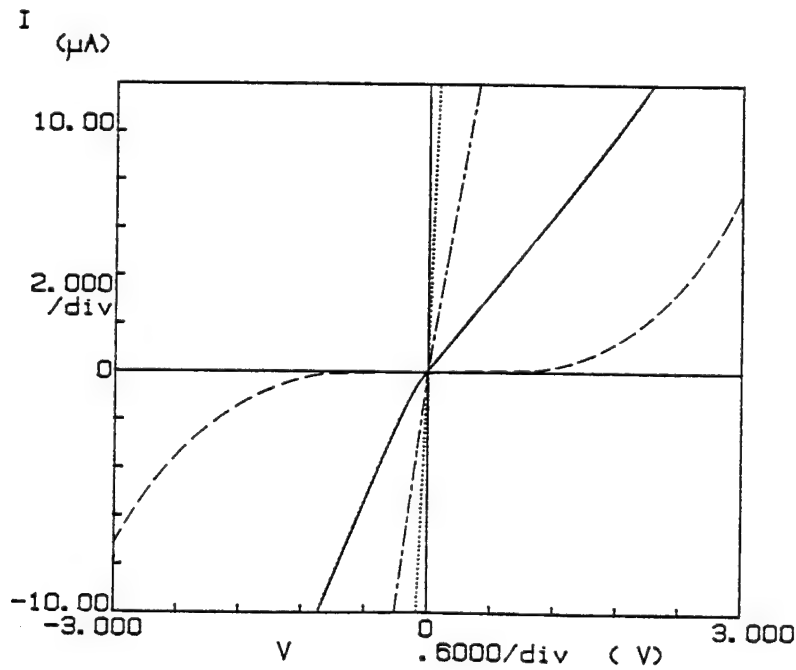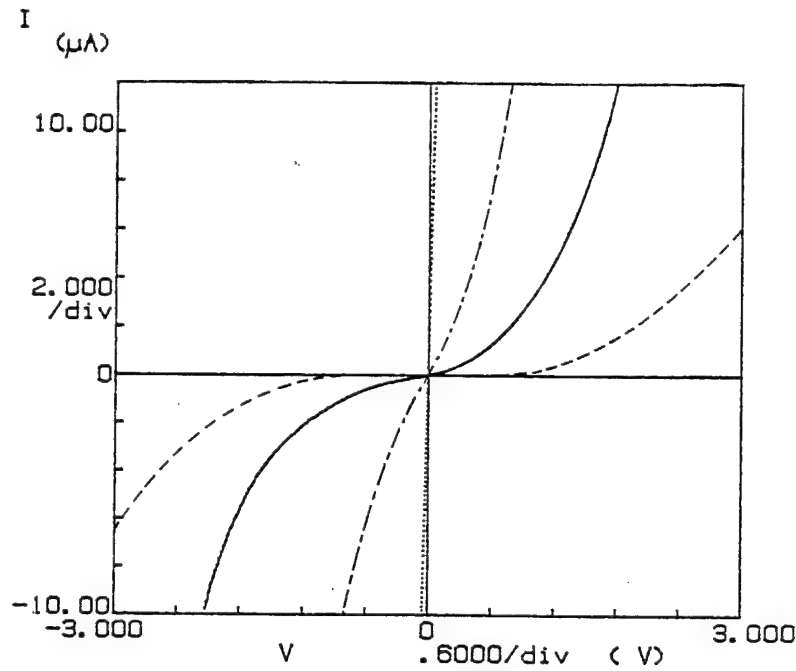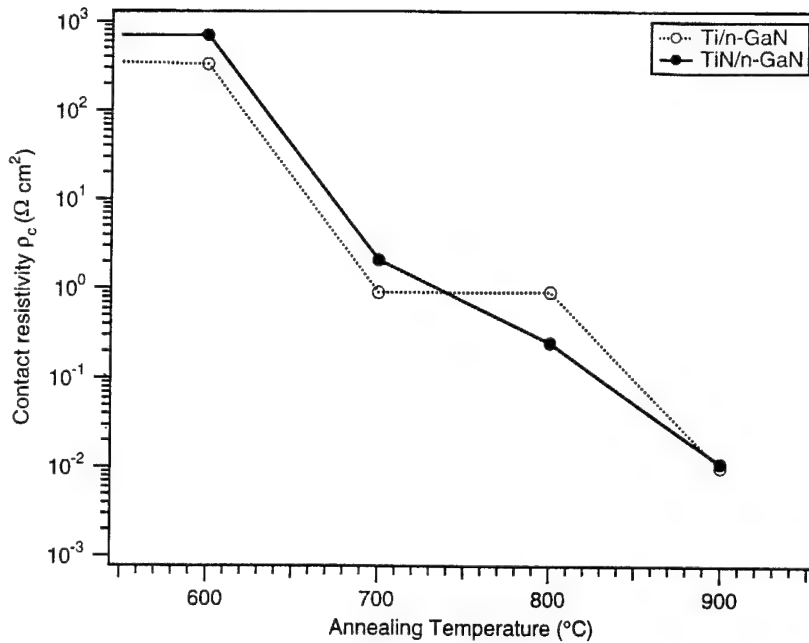f 2.5×10^{-5} $\Omega\cdot$cm^2. In contrast to the TiN contacts on the lower-doped GaN, the already low-ρ_c behavior did not change as a result of annealing treatment.

Room temperature TLM measurements showed that the ρ_c for both the Ti and TiN contacts decreased with increasing temperature, from 10^2 to the 10^{-2} Ω cm^2 range. These results are plotted in Fig. 4, showing ρ_c as a function of annealing temperature. Neither the Ti nor the TiN contacts changed substantially with respect to contact resistivity until the 700°C anneal. A large drop in ρ_c, of over two orders of magnitude, occurred after 700 °C and followed by smaller drops in ρ_c at higher temperatures.

Cu$_3$Ge Contacts on n-GaN:Si. Current-voltage measurements of the Cu$_3$Ge contacts on GaN:Si ($n=7.4\times10^{18}$ cm^{-3}) revealed nearly-linear ohmic behavior with low overall resistance; TLM measurements showed the ρ_c to be 4.9×10^{-3} $\Omega\cdot$cm^2. The same contact system deposited on lower-doped GaN ($n=4.5\times10^{17}$ cm^{-3}) was much more resistive and showed more non-linearity in the I-V measurements; a ρ_c of 18 $\Omega\cdot$cm^2 was obtained. In both cases, the as-alloyed contacts had a shiny, smooth surface, indicative of little or no roughening or reaction at the interface. Subsequent annealing of the samples under UHV conditions resulted in little change in ρ_c for both doping levels, until the samples were heated at 800°C. However, after the 600°C anneal, the I-V measurements of the contacts on the lightly-doped GaN

45

($n=4.5 \times 10^{17}$ cm^{-3}) became substantially more linear. After the 800°C annealing step, the Cu$_3$Ge ρ_c for both GaN doping levels increased sharply, as shown in Fig. 5. For the $n=7.4 \times 10^{18}$ cm^{-3} contacts, the ρ_c rose to 1.0 $\Omega \cdot$cm^2, and on the $n=4.5 \times 10^{17}$ cm^{-3} contacts the ρ_c reached 69 $\Omega \cdot$cm^2. In addition, the metal contact surfaces appeared somewhat dulled after the 800°C anneal, indicating that some roughening had taken place. Current-voltage measurements of the Cu$_3$Ge metal layers themselves revealed that the metal layers had become much more resistive as a result of the 800°C anneal. This increased series resistance in the measurement circuit was responsible for the increase in calculated ρ_c values.
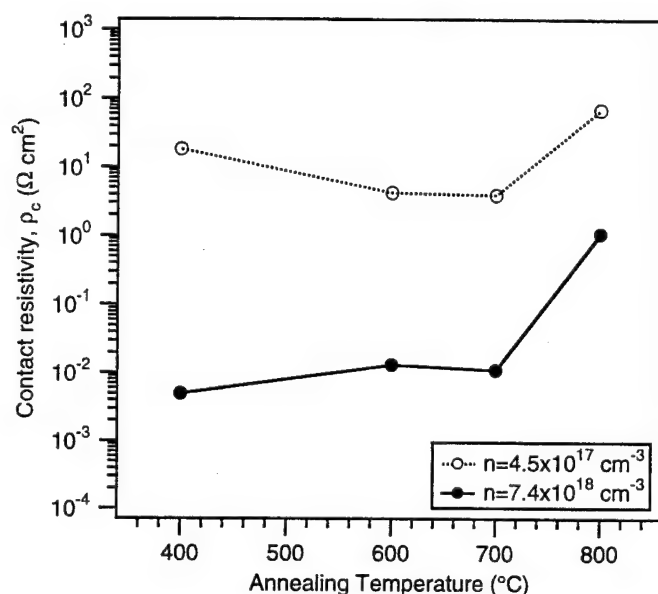
Figure 5.   Specific contact resistivity for Cu$_3$Ge/n-GaN:Si contacts as a function of annealing temperature.

Pt Contacts on p-GaN:Mg. These contacts were found to be quasi-ohmic and highly resistive in the as-deposited condition, as shown in Fig. 6. Upon annealing at temperatures up through 800°C, the I-V behavior of the Pt contacts became more linear and ohmic and resistances dropped. After the 900°C step, however, the contacts began to turn more resistive again. Associated with this increase in resistance was an increasingly dull appearance of the Pt metal surface, indicative of possible interfacial reaction.

D. Discussion

GaN Surface Cleaning. The presence of measurable amounts of O and C on all of the air-exposed surfaces is not surprising, given the fact that at atmospheric pressure, the time required to adsorb 1 monolayer is less than 10^{-9} s. Also, the use of UV/ozone oxidation on the

as-received surface resulted, not surprisingly, in a very large increase in O and a slight increase in C coverage. A very small Cl peak was observed as well. Trace amounts of possible Cl appear in the spectra from other samples as well, due perhaps to earlier cleaning treatments (>1 month prior to this study), from HCl or TCE, and/or chloride present as the predominant impurity in even high-purity HF solutions.
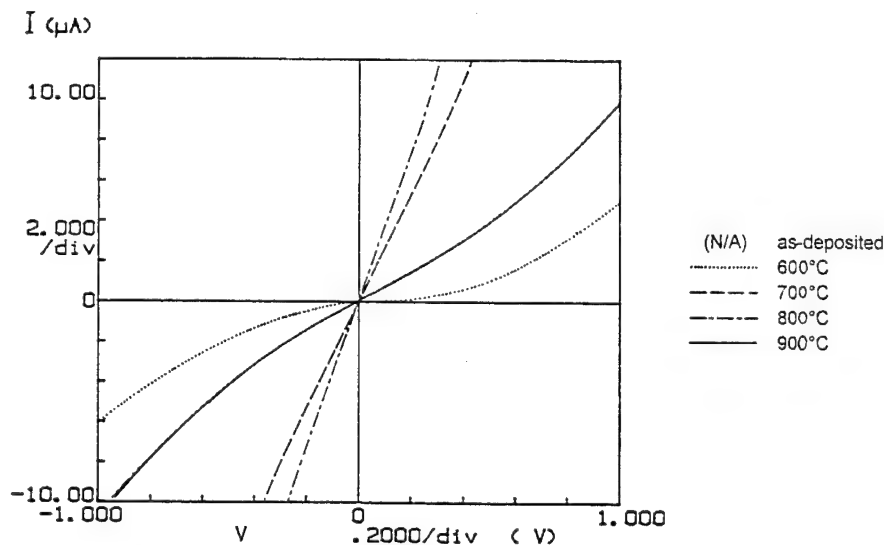

Figure 6.   Evolution of I-V behavior for Pt contacts on Mg-doped GaN as a function of annealing temperature.

Though the acid:MeOH-treated surfaces naturally exhibited higher C peak intensities before the thermal desorption, both the HCl:MeOH- and HF:MeOH-treated samples showed lower C peak intensities than the HCl:DI- and HF:DI-treated samples after the 800°C heating step. This observation is consistent with the expectation that the methanol is primarily physisorbed, and its occupation of many available surface sites protects the surface from coverage with more strongly bound C-containing species. This effect is much more pronounced with the HF cleaning than with the HCl; for both the HF:DI and HF:MeOH-cleaned surfaces, the C/N peak height ratios had diminished drastically after the 800°C heating step. This substantial difference in thermal desorption behavior supports the expectation that HF is more effective than HCl at passivating active sites on the surface—or at least sites active with respect to carbon bonding. On all of the samples heated to 800°C, a certain amount of the initial oxide coverage stubbornly refused to desorb. Approximately similar O/N signal intensities remained after the 800°C desorption, with the HF:DI-treated samples retaining somewhat more oxygen than the others.

The results of other recent thermal desorption experiments performed in vacuum on similar GaN films have so far shown that O and C do not completely disappear, even up to temperatures where GaN decomposition occurs (>800-900°C), unless an active species is

present to assist in surface removal, i.e., hydrogen plasma, ion bombardment, etc. Ingrey *et al.* reported the same phenomenon for InGaAs [33]. An important consideration in this regard is the current concern with the role of H and its compensation of acceptor impurities. The search for a method of obtaining surfaces as atomically "pristine" as possible must necessarily include the characterization of any surface damage or other property degradation that may occur in connection with surface cleaning procedures. The use of ionized, accelerated gas-phase species in cleaning methods is likely to cause some surface damage, depending on the kinetic energy and mass of the ionized species. In addition, there are indications that even short-term exposure to aqueous acid cleaning solutions can cause micro roughening of GaAs surfaces, which increases with time of exposure [34].

The relative increases of O and C before the 800°C analysis were different for the two cleaning treatments. While the C concentration on the HCl:DI surface remained approximately the same, the relative O signal more than doubled. On the HF:MeOH surface, the C signal increased while the O signal remained the same. In addition, there is some evidence that the C on the HCl:DI surface changed state prior to the 800°C analysis: it shows a different peak shape in that spectrum, while all the other spectra in this study exhibit the typical "aliphatic" C contamination peak shape. Assuming that the suspected contamination of the samples involved both O and C, the differences between the samples may reflect different types of surface passivation or protection against further surface coverage. The larger amount of C-containing surface coverage on the HF:MeOH-treated GaN may have served to protect against subsequent oxidation, as described in Ingrey's work on III-V surface cleaning [13], while the essentially cleaner HCl:DI-treated surface lacked such protection. Overall, the HCl:DI treatment produces the cleanest surfaces observed to date, both with and without subsequent thermal desorption. The possible additional protection offered by the HF:MeOH treatment may be useful for longer-term storage of GaN films, depending on the methods used for further cleaning.

Ti and TiN Contacts on n-GaN:Si. TiN is metallic in electrical behavior, in contrast to the insulating nitride formed by Al. Both AlN and TiN have highly negative free energies of formation and are therefore thermodynamically favored. As described in the preceding section, the nitridation of Al at the contact interface results in increasing resistivity. By comparison, the formation of metallic TiN at the contact interface is expected to improve contact characteristics; a substantial decrease in ρ_c as a function of annealing was indeed observed. The role of Ti nitridation in the formation of low-resistivity Ti-containing contacts to n-GaN has been discussed by Lin *et al.* [20]. The results of the present study indicate that high-temperature annealing benefits both Ti and TiN contacts. The roles played by microstructural changes and loss of N from the GaN at high temperatures are being investigated by means of cross-sectional, high-resolution TEM analysis that is currently underway.

Both Ti and TiN are low work function metals with TiN having the lower value (ϕ_{Ti}=4.1 eV, ϕ_{TiN}=3.74 eV), and thus according to the Schottky-Mott-Bardeen model should be more likely to form ohmic contacts to n-type semiconductors. In addition, there are reasons to expect that both Ti and TiN might deposit epitaxially on GaN and AlN, as they both do on 6H-SiC [35,36]. Titanium has a hexagonal structure and a basal-plane lattice parameter (a_{Ti}=2.951 Å, a_{Hf}=3.195 Å) similar to that of SiC, GaN and AlN (a_{SiC}=3.08 Å; a_{GaN}=3.189 Å; a_{AlN}=3.112 Å). TiN has the NaCl structure and has a reasonably close lattice match to hexagonal GaN (-5.9 %) and AlN (-3.6 %) in the close-packed (111) planes. TiN is thermally very stable and highly resistant to oxidation, forming only a thin passive oxide film on the surface. Though Ti oxidizes readily, it too forms only a thin passive film on the surface under normal conditions, and has a high melting point.

The Ti and TiN were deposited at the same temperature to the same thickness (1000 Å) on similar GaN:Si films. The primary difference between the two metal depositions is the presence of extra available N during TiN growth to fully bond with the Ti. In TiN the Ti becomes stoichiometrically nitrided and strongly bound to N, whereas in the case of Ti alone, any Ti nitride formation that takes place must derive its nitrogen from the GaN. The nitridation of Ti is thermodynamically favored with respect to GaN: the Gibbs free energy of formation ΔG_f^0 for TiN at 298 K is -6309.2 kJ/mol, while ΔG_f^0 for GaN is only -77.8 kJ/mol. The difference in ΔG_f^0 between the two does not change appreciably through 1000 K. The removal of Ti from the GaN would result in N vacancies, which are widely believed to function as shallow donors in GaN. M.E. Lin and H. Morkoç et al. have estimated that 2 monolayers of TiN formation at a contact interface is sufficient to form a 10 nm surface layer of GaN having an electron density of 10^{20} cm^{-3} through which electrons could efficiently tunnel, thus greatly increasing the current-carrying capacity of the contact interface [20,37].

The TiN contacts deposited on these GaN:Si films (n=1.2×10^{18} cm^{-3}) did not show the low-resistance behavior exhibited by the as-deposited TiN contacts on more highly doped GaN:Si (n=9.4×10^{18} cm^{-3}) described in the preceding 1994 Annual Report (December 1994). This difference in GaN carrier concentration may account for much of the difference in ρ_c behavior. Overall, the Ti and TiN contacts in this experiment behaved similarly with respect to annealing treatment—possibly for different reasons. The TiN has a lower work function and thus may produce a lower barrier than Ti on GaN, but the un-nitrided Ti is able to create N vacancies in the GaN interfacial region, which would also result in improved contact behavior. More detailed study of this contact system, especially high-resolution microstructural characterization via X-TEM to look for epitaxial relationships and any compositional changes that take place, is planned to help understand the current transport mechanisms and establish the utility of this contact system for high-temperature device applications.

49

CuGe Contacts on n-GaN:Si. As described above, the Cu_3Ge contacts exhibited ohmic behavior on both lightly-doped ($n=4.5\times10^{17}$ cm^{-3}) and heavily-doped ($n=7.4\times10^{18}$ cm^{-3}) n-GaN:Si films. This behavior was observed in both the as-alloyed contacts, alloyed in vacuum at 400°C, and contacts annealed in vacuum through 800°C. The annealing treatments were intended to increase the donor concentration at the contact interface by means of Ge diffusion into the GaN. A reduction of ρ_c was not seen as a result of the annealing treatments up through 700°C, indicating that little transport of Ge into the GaN took place at these temperatures. The increase in ρ_c that occurred after the 800°C anneal was a result of degradation of the metal layer itself. In the as-alloyed state, the metal layer exhibited low-resistivity properties; after the 800°C anneal the probe-to-probe resistance of the metal layer had increased dramatically and overwhelmed all other electrical effects contributing to the I-V measurements used for TLM calculations.

Since the Cu_3Ge ϵ_1 phase melts completely at 747°C, the changes in metal properties are most likely due to its melting and cooling. The reason for heating the metal contact layer above its melting point is drawn from the industry's experience with the familiar Au-Ge ohmic contacts on n-GaAs, which are annealed at temperatures above the Au-Ge alloy melting point to achieve ohmic behavior. However, the best results with Au-Ge contacts are achieved when the Au-Ge alloy is capped with a thin layer of Ni and then a thick low-resistivity overlayer of Au. Also, it is now known that the Ni layer, originally added to keep the liquid Au-Ge metal from "balling up" on the GaAs surface during alloying, actually participates in the contact alloying process in an extensive and complex way. Far from being a neutral, refractory capping layer, the Ni has been found to alloy extensively and to enhance the interdiffusion of the interface constituents, even at the relatively low temperatures used for this contact system (~425°C) [2]. In an analogous way, it may be possible to obtain better performance from the Cu_3Ge/n-GaN contact system if capping layers or other processing parameters can be adjusted to protect the metal from degradation at high temperatures. Also, it may be possible to enhance the GaN contact interface with Ge and thus improve ρ_c by annealing the contacts at longer times at temperatures below the melting point.

Pt Contacts on p-GaN:Mg. Platinum is a very high work function metal (ϕ_{Pt}=5.65 eV) and thus provides a favorable band offset for minimizing the Schottky barrier to a p-type semiconductor. In addition, Pt is thermally very stable and highly resistant to oxidation. In the preceding annual report for this project (December 1994), linear ohmic behavior and very low ρ_c was observed for as-deposited Pt contacts to Mg-doped GaN. Investigation of Pt as an ohmic contact candidate for p-type GaN was conducted earlier in this study, as described in the semiannual report for June 1993, but the results were not as promising at that time. Substantial improvements in GaN film quality and electrical properties have been made since then. The newer GaN:Mg described here were grown by MOVPE instead of MBE, as was the case when

the earlier study was conducted. The measurement of carrier concentration and mobility via Hall measurements has been difficult for p-type GaN so far, due to inconsistent and high-resistance ohmic contact behavior.

The work of Sands *et al.* [38,39] has shown that extensive interfacial reaction can occur between Pt and GaAs, due to metallurgical reactions involving both Ga and As. Though lacking the mobile and reactive As species, GaN nevertheless has shown the ability to react with noble metals when annealed at high temperature, as described in the preceding annual report in connection with Au contacts on p-GaN. Thus, changing behavior of the Pt contacts as a function of annealing temperature is not surprising. The increasing resistance seen for the 900°C anneal is likely due to a progression of interfacial phase formation. Upcoming cross-sectional microstructural characterization will provide additional information and aid in the understanding of the behavior of this contact system.

E.   Conclusions

The results of surface cleaning experiments conducted in this study so far has shown that HCL:DI (1:1) solution cleaning produces the cleanest surfaces of all the wet chemical cleaning methods yet examined on GaN films, particularly if the wet cleaning is followed by a thermal desorption to at least 625°C. All of the cleaning methods examined that involved HF were found to leave more O and C on the surface in general, though there was some evidence that the HF:MeOH treatment might protect a GaN surface from further oxygen coverage. As yet, complete removal of O and C from air-exposed GaN surfaces has not been seen, even up to temperatures where GaN decomposition occurs (>800-900°C), unless an active species is present to assist in surface removal, i.e., hydrogen plasma, ion bombardment, etc.

The comparison of Ti and TiN contacts on similarly-doped n-GaN has shown them to behave similarly with respect to the effects of annealing on the specific contact resistivity. In both cases, the ρ_c dropped significantly as a result of annealing through 900°C. It is likely that the improvement in the behavior of the Ti contact system is due to the formation of TiN at the GaN interface, accompanied by loss of N in the form of N vacancies in the GaN. In the case of TiN, the improvement in behavior as a result of annealing may also be due to the loss of N from the interfacial region of the GaN. The TiN compound can exist over a range of stoichiometry and can thus accommodate a certain amount of additional N lost from the GaN at the high annealing temperatures, which would again increase the donor concentration at the contact interface. More detailed study of this contact system, especially high-resolution microstructural characterization via X-TEM to look for epitaxial relationships and any compositional changes that take place, is planned to help understand the current transport mechanisms and establish the utility of this contact system for high-temperature device applications.

As was the case with the TiN/n-GaN contacts, the ρ_c varied dramatically with the carrier concentration of the GaN studied. There was no significant improvement in ρ_c as a result of post-deposition annealing, though in the case of Cu_3Ge contacts on lightly-doped GaN the I-V behavior became substantially more linear after annealing at 600°C. The Cu_3Ge metal layers deteriorated as a result of annealing them at temperatures above the metal's melting point. High temperatures (above 700°C) may be necessary to drive Ge diffusion into the GaN to provide increased donor concentrations at the contact interface, but the melting of the Cu_3Ge metal and consequent degradation of its properties may make this difficult. Annealing the contacts for longer times at temperatures below the melting point may improve their performance. It may also be possible to preserve the integrity of the Cu_3Ge metal during high-temperature annealing through the use of capping layers or other adjustments of processing parameters.

Annealing studies of sputtered Pt contacts on Mg-doped GaN have shown an improvement in current-carrying behavior as a result of annealing, though a deterioration in performance was observed for the highest annealing temperature (900°C). The achievement of low-resistivity ohmic contacts to p-GaN is a necessary component for the development and application of many types of GaN-based devices. Further characterization of contact candidates for p-type material, including microstructural information obtained from X-TEM analysis, will yield greater understanding of the chemical and structural contributions to contact behavior and will allow more rapid and knowledgeable development of improved contact schemes and their capabilities.

F. References

1. T. C. Shen, G. B. Gao, H. Morkoç, J. Vac. Sci. Technol. B **10** (5) 2113 (1992).
2. R. Williams, *Modern GaAs Processing Techniques* (Artech House, Norwood, MA, 1990).
3. M. Murakami, Materials Science Reports (5) 273 (1990).
4. A. Piotrowska and E. Kaminska, Thin Solid Films **193/194** 511 (1990).
5. A. Piotrowska, A. Guivarc'h and G. Pelous, Solid-St. Electron. **26** (3) 179 (1983).
6. V. L. Rideout, Solid-St. Electron. **18** 541 (1975).
7. K. Tanahashi, H. J. Takata, A. Otsuki and M. Murakami, J. Appl. Phys. **72** (9) 4183 (1992).
8. H. C. Hugon, B. Agius, F. Varniere, M. Froment and F. Pillier, J. Appl. Phys. **72** (8) 3570 (1992).
9. H. J. Takata, K. Tanahashi, A. Otsuki, H. Inui and M. Murakami, J.Appl. Phys. **72**(9) 4191 (1992).
10. W. O. Barnard, G. Myburg and F. D. Auret, Appl. Phys. Lett. **61** (16) 1933 (1992).
11. G. Stareev, Appl. Phys. Lett. **62** (22) 2801 (1993).
12. E. D. Marshall and M. Murakami, in *Contacts to Semiconductors,* edited by L. J. Brillson (Noyes, Park Ridge, NJ, 1993).
13. S. Ingrey, J. Vac. Sci. Technol. A **10** (4) 829 (1992).
14. F. W. Ragay, M. R. Leys and J. H. Wolter, Appl. Phys. Lett. **63** (9) 1234 (1993).
15. H. K. Henisch, *Semiconductor Contacts.* (Clarendon Press, Oxford, 1984).
16. E. H. Rhoderick and R. H. Williams, *Metal-Semiconductor Contacts* (Oxford University Press, New York, 1988).

17. S. Kurtin, T. C. McGill and C. A. Mead, Phys. Rev. Lett. **22** (26) 1433 (1969).
18. J. S. Foresi, *Ohmic Contacts and Schottky Barriers on GaN,* M.S. Thesis, Boston University (1992).
19. J. S. Foresi and T. D. Moustakas, Appl. Phys. Lett. **62** (22) 2859 (1993).
20. M. E. Lin, Z. Ma, F. Y. Huang, Z. F. Fan, L. H. Allen, and H. Morkoç, Appl. Phys. Lett. **64** (8) 1003 (1994).
21. B. L. Crowder and S. Zirinski, IEEE Trans. Electron Devices **ED-26**, 369 (1979).
22. S. C. Binari, H.B. Dietrich, and G. Kelner, Electronics Lett. **30**(11) 909 (1994).
23. S. P. Murarka, *Silicides for VLSI Applications,* Academic Press, New York (1983).
24. L. Krusin-Elbaum, J. Y.-C. Sun, and C.-Y. Ting, IEEE Trans. Electron Devices **ED-34**, 58 (1987).
25. J. C. Hensel, R. T. Tung, J. M. Poate, and F. C. Unterwald, Appl. Phys. Lett. **44**, 913 (1984); Phys. Rev. Lett. **54**, 1840 (1985).
26. P. H. Woerlee, P. M. Th.M . van Attekum, A. A. M. Hoeben, G. A. M. Hurkx, and R. A. M. Wolters, Appl. Phys. Lett. **44**, 876 (1984).
27. M. T. Huang, T. L. Martin, V. Malhotra, and J. E. Mahan, J. Vac. Sci. Technol. B **3**, 836 (1985).
28. L. Krusin-Elbaum and M. O. Aboelfotoh, Appl Phys. Lett. **58**(12) 1341 (1991).
29. M. O. Aboelfotoh, H. M. Tawancy, and L. Krusin-Elbaum, Appl. Phys. Lett. **63**(12) 1622 (1993).
30. M. O. Aboelfotoh, K. N. Tu, F. Nava, and M. Michelini, J. Appl. Phys. **75**(1) (1994).
31. M. O. Aboelfotoh, H. M. Tawancy, J. Appl. Phys. **75**(4) (1994).
32. G. K. Reeves and H. B. Harrison, IEEE Electron Device Lett. **EDL-3** 111 (1982).
33. S. Ingrey, W. Lau, and R. Sodhi, J. Vac. Sci. Technol. A **7**, 1554 (1989).
34. D. E. Aspnes and A. A. Studna, Appl. Phys. Lett. **46** (11) 1071 (1985).
35. L. M. Porter, R. F. Davis, J. S. Bow, M. J. Kim, R. W. Carpenter, and R. C. Glass, J. Mater. Res., **10** (3) 668 (1995).
36. R. C. Glass, Ph.D. thesis, North Carolina State University, June 1993.
37. H. Morkoç, S. Strite, G. B. Gao, M. E. Lin, B. Sverdlov, and M. Burns, J. Appl. Phys. **76** (3) 1363 (1994).
38. T. Sands, V. G. Keramidas, A.J. Yu, K-M. Yu, R. Gronsky, and J. Washburn, J. Mater. Res. **2** (2) 262 (1987).
39. T. Sands, V. G. Keramidas, K-M. Yu, J. Washburn, and K Krishnan, J. Appl. Phys. **62** (5) 2070 (1987).

VII. Distribution List

Mr. Max Yoder   3
Office of Naval Research
Electronics Division, Code: 312
Ballston Tower One
800 N. Quincy Street
Arlington, VA 22217-5660

Administrative Contracting Officer   1
Office of Naval Research
Regional Office Atlanta
101 Marietta Tower, Suite 2805
101 Marietta Street
Atlanta, GA 30323-0008

Director, Naval Research Laboratory   1
ATTN: Code 2627
Washington, DC 20375

Defense Technical Information Center   2
Bldg. 5, Cameron Station
Alexandria, VA 22314

Washington Headquarters Services   2
ATTN: Dept. Acctg. Division
Room 3B269, The Pentagon
Washington, DC 20301-1135